Chapter 12
Particle Tribology: Granular, Slurry, and Powder Tribosystems

C. Fred Higgs III, Martin Marinack Jr., Jeremiah Mpagazehe, and Randyka Pudjoprawoto

Abstract The purpose of this chapter is to give the reader a basic understanding of particles in sliding contact. First, we will describe granular flows (the flow of inelastic particles that transfer momentum primarily through collisions) from a tribology perspective, including modeling and experiments that have been conducted inside and outside of the tribology community. Second, slurry flow (particles in gas or liquids) tribosystems will be discussed including models and experiments related to the flow of particles in fluids. And finally, we conclude with a section on powder lubrication (soft particles which coalesce under load and coat surface asperities), where thick and thin film powder lubrication is discussed along with select modeling and experimental approaches.

1 Introduction

Particles in sliding contacts have always been a complex area of tribology. While tribology is a very broad field that is diffused into many areas of engineering and science, gaining an understanding of the interface between two sliding materials (i.e., a tribosystem) requires one to take a multidisciplinary perspective. When particles are introduced into the interface, the problem can quickly become intractable and thus highly empirical to compensate for the uncertainties involved with predicting the resulting tribology. Further, various particle flow communities are independent fields of science and engineering themselves, so few tribologists are trained to interpret the behavior of particulate systems and few classical particle engineers are trained to understand phenomena associated with sliding surfaces and the inherent friction, wear, and/or lubrication phenomena that emerge. For example, classical granular flow is a field mostly comprised of chemical engineers and

C.F. Higgs III (✉) • M. Marinack Jr. • J. Mpagazehe • R. Pudjoprawoto
Carnegie Mellon University (CMU), Pittsburgh PA, USA
e-mail: higgs@andrew.cmu.edu

P.L. Menezes et al. (eds.), *Tribology for Scientists and Engineers: From Basics to Advanced Concepts*, DOI 10.1007/978-1-4614-1945-7_12,

physicists; the mechanical engineer studying the flow of these inelastic grains is rarer, albeit not uncommon. The same situation exists with the flow of particles in fluids in sliding contacts, which we call slurry tribology. There is a strong slurry community, more commonly known as the multiphase flow community, which exists primarily to study fossil fuel-type energy systems such as circulating fluidized beds and flowing coal particles. This community routinely solves Navier–Stokes equations, not just for the fluid phase but for the solid phase comprised of flowing particles as well. The same cannot be said of powder lubrication however. Powder flows in sliding contacts remain an area rooted in tribology, and unlike granular and slurry (multiphase) flows, researchers outside of tribology reference papers within tribology journals when studying problems involving powders in sliding contacts. Even in areas such as earthquake science, powder lubrication works found in tribology journals are referenced to describe intriguing friction phenomena connected to shearing layers of earth.

2 Granular Flow Tribology

Granular flows are complex flows of solid, macroscopic, non-cohesive particulates (or granules), which collectively comprise the bulk flow. These granules are generally on the order of millimeters (mm) or larger, unlike powder flow particles (discussed in Sect. 4) which generally reside on the order of micrometers (μm). Granular flows are often characterized by the fact that they dissipate energy (unlike traditional liquid-based flows) through the inelastic collisions and interactions between the individual grains comprising the global flow. Granular flows can exhibit solid-, liquid-, and gaseous-like behavior under varying flow conditions. This display of nonlinear and multiphase flow behavior makes the prediction and study of granular flows challenging both locally (at the individual particle scale) and globally (at the bulk flow scale).

In tribology, liquid lubricants break down at extreme temperatures and can bring about stiction in micro-/nanoscale environments. This has led to the advent of alternative, dry lubrication mechanisms such as powder and granular flow. While powder tribology is described in detail in Sect. 4, the focus of this section remains granular tribology. Granular flow tribology focuses on the study of granular flows between relative sliding contacts, specifically focusing on the use of granular flows as a lubricant. Granular flows have been proposed as a particulate lubricant alternative to traditional oil-based lubricants [1–3] because of their hydrodynamic fluid behavior in sliding contacts, specifically their ability to carry loads and accommodate surface velocities. Typical sliding contact geometries, as summarized in Wornyoh et al. [4], include annular, parallel, and converging geometries, as shown in Fig. 12.1.

In their detailed review of dry particulate lubrication, Wornyoh et al. [4] define granular lubricants as “dry, ‘cohesionless,’ hard particles that essentially maintain their spherical geometry under load and accommodate surface velocity differences through sliding and rolling at low shear rates, and largely through collisions at high

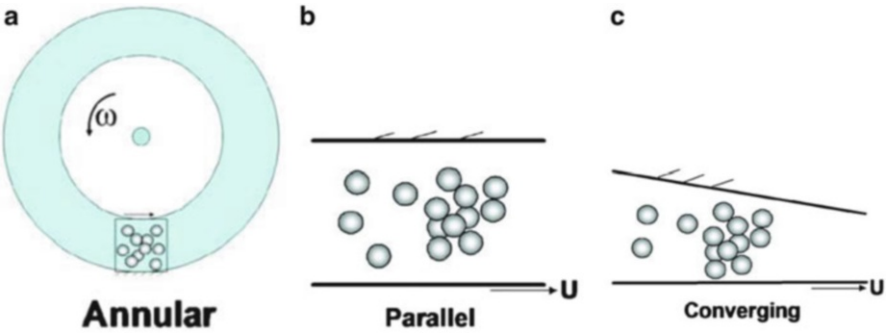

Fig. 12.1 Sliding contact geometries: (**a**) Annular, (**b**) parallel, and (**c**) converging [4]

shear rates." In sliding contact geometries, granular lubrication mechanisms have shown that the particles inside the contact can enhance lubrication and lower friction beyond boundary lubrication levels. Granular flow lubricants also show a density distribution in sliding contacts, where a low-density region exists near the surfaces, while a high-density region exists near the center of the flow. Unlike hydrodynamic fluids, granular flow lubricants display a load-carrying capacity in static and parallel sliding (dynamic) contact regions, as well as a significant (measurable) amount of slip at the boundaries of macroscale geometries [4]. As an example of a specific granular lubrication application, McKeague and Khonsari [5] developed a model which predicts the behavior of a granular flow inside of a slider-bearing geometry.

Two modes of granular lubrication have been observed to exist. At lower shear rates or high loads, the load is supported by strong contact forces between compacted granules. This regime is known as granular *contact* lubrication; the classical granular flow community calls this the frictional regime. Global frictional forces are due to the continuous shearing of the beads, and the load-carrying capacity is due to elastic and plastic deformation of the granules in contact. At increased shear rates or small loads, the granules are more agitated and lubrication in this secondary regime is known as granular *kinetic* lubrication. There is also a *transition* regime which may be quasi-static [6, 7]. Load-carrying capacity in this mode is due to the shear and normal forces created by the colliding particles against the upper surface.

The scope of granular flows in tribology is not limited to the study of granular lubrication. Granular flow tribology also involves the more general examination of the role of friction, macroscale surface roughness, and the collision and contact mechanics of moving particles. Particularly important in characterizing and understanding granular flows from both a classical and tribological perspective is the study of the individual particles which comprise the bulk granular flow. This involves the study of individual particle collision parameters such as the coefficient of friction (COF) and coefficient of restitution (COR). Knowledge and understanding of all of these granular flow concepts (friction, roughness, contact

mechanics, COF, COR, etc.) can provide insight into areas, industries, and applications well beyond granular lubrication, including solids processing [8], pharmaceuticals [9], wheel and granular terrain interaction of planetary rovers [10], coal transportation [11], granular segregation [12, 13], and the design and operation of hoppers [14, 15] and silos [16, 17].

The following sections examine numerous aspects of granular flow tribology, beginning with a look at applications and phenomena such as segregation, jamming, and planetary rover–terrain interaction. Also discussed are key experimental geometries used to elucidate core granular flow science. This includes the study of individual particle physics as well as the study of global granular flow properties. Finally, modeling techniques in the study of granular flows are discussed, which includes an examination of both discrete (discrete element method (DEM), cellular automata (CA), and finite element method (FEM)) and continuum modeling approaches. Before moving forward, it should be noted that this section should not be viewed as an exhaustive examination of granular flows in tribology. Instead, it serves as a detailed overview of the major areas of study, concepts, experimental methods, and modeling methods in the study of granular flow tribology.

2.1 Applications and Phenomena

Granular flows display several unique behaviors and physical phenomena. Granular flow lubrication, which was already discussed in the granular introduction, is one such phenomenon. Other common granular flow phenomena include granular segregation and jamming, both of which are often witnessed in solids processing applications involving hoppers, silos, and/or mixers. Another interesting granular flow behavior involves the shear flow witnessed beneath a planetary rover wheel as it interacts with the granular terrain. The following section will highlight and discuss these three phenomena (segregation, jamming, and planetary rover-terrain interaction) in further detail.

It is well known that even small variations in granular properties and/or characteristics can lead to segregation in a granular flow. Granular segregation involves the separation (“unmixing”) of individual granular species inside of a bidisperse or polydisperse flow (i.e., a flow with two or more species). Bi/polydispersity in a granular flow can be due to differences in any number of granule properties or characteristics such as size, shape, material density, restitution, and friction coefficient. While granular flow segregation can be induced by variations in any number of these characteristics, perhaps the most prevalent characteristic inducing granular segregation is particle size. Ottino and Khakar [18] provide a detailed review of studies examining both density and size segregation for a range of granular flow geometries and situations. Particle size segregation is studied and witnessed in a wide variety of natural processes and industrial applications. Natural processes, such as avalanches, were studied by Gray and Ancey [19] who demonstrated that in an avalanche flow, the larger particles

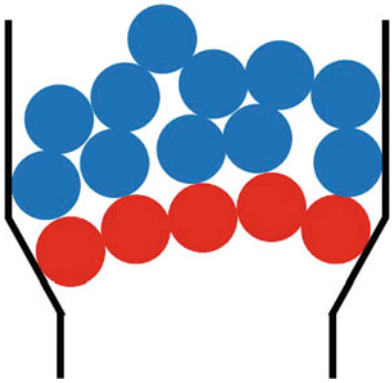

Fig. 12.2 Schematic of a two-dimensional hopper exhibiting a jammed configuration (adapted from To et al. [15]). The *red* granules at the *bottom* display the formation of a granular arch which causes jamming of the flow

segregate at the top, where the flow velocity is largest, and move towards the flow front [19]. In terms of industrial applications, size segregation is displayed and has been studied in hoppers [20, 21] and silos [16, 22], as well as mixers [23], each of which is used extensively in the solids processing industries (e.g., pharmaceuticals and food processing).

Maintaining a tribological perspective, size segregation is a phenomenon which is also seen extensively in granular shear flows, such as those exemplified by the geometries shown in Fig. 12.1. Size segregation in a parallel-type geometry (Fig. 12.1b) has been studied extensively by Golick and Daniels [13] and May and her colleagues [12, 24]. In the work of Golick and Daniels [13], a bidisperse flow using glass particles with diameters of 4 and 6 mm was initially placed between two disks such that the smaller particles resided at the top, while the larger particles resided at the bottom. As the flow was sheared between parallel disks, the larger particles began to segregate to the top creating a mixed flow for a period of time. However, by the end of the experiment, the flow was fully segregated, with the larger particles now residing at the top of the flow and the smaller particles at the bottom. This classic trend of larger particles segregating to the top occurs because the smaller particles tend to fall through the gaps between the large particles in a sievelike fashion.

Jamming is another relevant and important granular flow phenomenon which has been studied extensively in the literature [15, 25–31]. Jamming involves the granular flow becoming rigid and stagnating. Figure 12.2, adapted from the work of To et al. [15], shows an example of jamming occurring inside of a hopper flow. At the local level, jamming is related to the forces and force distribution among the individual particles and particle chains [26–28]. Jamming in granular flows has been likened to the jamming of certain other complex fluids like glass which is rigid (jammed) but can transition to a flowing state at higher temperatures [26]. Granular flows have likewise demonstrated the ability to transition between a flowing state and a jammed (stagnate) state based on the properties of the so-called granular temperature, solid fraction, and shear stress, as exemplified in the works of Zhang et al. [28] and Liu and Nagel [31].

A third granular flow application is the interaction between planetary rover wheels and granular regolith (terrain). As described by Higgs et al. [10], wheeled

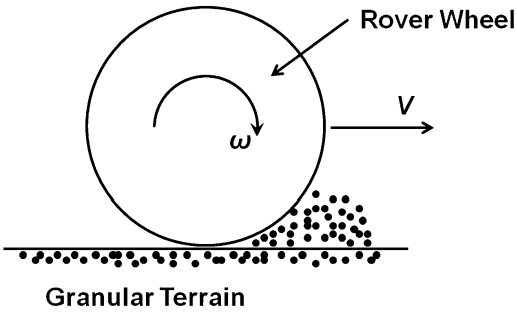

Fig. 12.3 Schematic of the planetary rover wheel–terrain interaction geometry, showing the individual granules becoming entrained in the converging gap at the wheel's leading edge (adapted from [33])

mobile robots, also known as rovers, are the primary vehicles for transporting scientific instrumentation across rough planetary terrain while being controlled remotely. Since there is a finite lifetime for which scientific information can be obtained, it is important that the rovers are reliably built to transverse the rough terrain without mechanical failure [10]. One of the most important mechanical operations of the rover is the ability of the rover wheel to negotiate the granular-type Martian surface, which requires sufficient traction between the wheel surface and granular terrain [10]. The planetary rover wheel and granular terrain display a geometry which is detailed in the works of Shibly et al. [32] and Liu et al. [33]. Figure 12.3 (adapted from Liu et al. [33]) displays a schematic for a rover wheel being driven on a granular surface in which the granular material enters the converging gap at the front end of the driven wheel [33]. The key thing to notice from the diagram in Fig. 12.3 is that the geometry of the rover wheel–terrain interaction is that of a converging-type sliding contact as depicted in Fig. 12.1c. Thus, this application/phenomenon becomes a granular flow tribology problem in that the wheel–terrain interface serves as a converging gap flow bounded by the wheel on one side and the bulk granular material on the other. This situation also shows the development of different granular flow regimes at different locations. The portion of the granules near the surface flows due to the shear being applied by the wheel, while the base of the granular terrain remains stationary. A more detailed summary and review of specific theoretical, simulation, and experimental work performed on wheel–terrain interaction mechanics for planetary rovers can be found in the work of Ding et al. [34].

2.2 Experiments

2.2.1 Single-Particle Experiments: Coefficient of Restitution

Granular flow experimentation takes place at both the single-particle (microscopic) level and the global (macroscopic) bulk flow level. At the single-particle level, individual particle and collision properties are examined, as these properties

ultimately drive the behavior of the bulk flow. Granular collision properties, such as coefficient of restitution (COR) and coefficient of friction (COF), are of particular importance, as they influence the granular flow characteristics, such as velocity, spin, solid fraction, and granular temperature. The following section details the experimental examination of the COR. COF is studied through the use of pin-on-disk testing of individual granules to characterize friction inside of granular flows.

The coefficient of restitution (COR) is a parameter which defines the ratio of relative post-collision velocity to pre-collision velocity when two materials collide. Mathematically, the coefficient of restitution between colliding materials can be written as seen in (12.1), where e, $v_{reb,1}$, $v_{reb,2}$, $v_{imp,2}$, and $v_{imp,1}$ represent the COR, the rebound velocity of object 1, the rebound velocity of object 2, the impact velocity of object 2, and the impact velocity of the object 1, respectively:

$$e = \frac{v_{reb,1} - v_{reb,2}}{v_{imp,2} - v_{imp,1}} \tag{12.1}$$

The coefficient of restitution can also be understood to indicate the fraction of the pre-collision kinetic energy present after the collision, where $e = 1$ represents a perfectly elastic collision with no kinetic energy loss and $e = 0$ represents a perfectly inelastic collision where all kinetic energy is dissipated during the collision. When examining the COR as it relates to granular flows, several collision cases (geometries) are of significant importance.

The first of these cases is granules (spheres) colliding with thick plates (blocks) and thin plates, which represent the boundaries of many granular systems. In the case of sphere–plate collisions, most of the experimental rigs are relatively simple in their construction and design, with spheres being dropped (under the influence of gravity) on a plate [35–39]. In these setups, the plates (like most granular boundaries) remain stationary (in the normal direction) during the collision. Thus, the expression in (12.1) can be reduced to that of (12.2). The subscripts in (12.2) are dropped since both values are now for the moving sphere, which impacts and rebounds from its collision with the plate/block:

$$e = \frac{-v_{reb}}{v_{imp}} \tag{12.2}$$

When the sphere (granule) is undergoing free fall under the influence of gravity, it is often useful to write the COR in terms of the impact (H_I) and rebound (H_R) height of the sphere for post-processing purposes. Through the use of kinematics and the inclusion of air drag effects, (12.2) can be written as (12.3), where the coefficient of restitution is now a function of heights instead of velocities. In (12.3), g, m_s, $F_{D,I}$, and $F_{D,R}$ represent the acceleration due to gravity, mass of the sphere, the drag force during the particle's free fall before impact, and the drag force during the particle's rebound to its maximum height, respectively:

$$e = \left(\sqrt{\frac{g + \left(\frac{F_{D,I}}{m_s}\right)}{g - \left(\frac{F_{D,R}}{m_s}\right)}} \right) \sqrt{\frac{H_R}{H_I}} \tag{12.3}$$

However, in most instances air drag effects can be neglected. This eliminates the first term in (12.3), reducing the coefficient of restitution equation (for a falling sphere impacting a stationary boundary) to the much simpler expression shown in (12.4):

$$e = \sqrt{\frac{H_R}{H_I}} \tag{12.4}$$

A large body of experiments has been performed to examine the coefficient of restitution between spheres and stationary plates. Tabor [40], Kharaz and Gorham [37], and others [38, 39, 41] performed experiments studying the coefficient of restitution between spheres and thick plates (large blocks) for various material combinations and impact velocities. Results from the work of Kharaz and Gorham [37], for 5 mm (diameter) aluminum oxide particles colliding against thick steel and aluminum plates, show a decrease in coefficient of restitution with increased impact velocity. This trend is well documented in other experimental works [36, 39, 40] as well as in theory development. For example, K.L. Johnson [42] developed an analytical formulation of e, for the plastic impact of rigid small spheres colliding with elastic–plastic bodies (i.e., blocks, spheres) at what the author termed "moderate" speeds (up to ~500 m/s). This formulation is shown in (12.5), where p_d, E^*, v_{imp}, and R represent the dynamic pressure (hardness) of the softer material, the composite elastic (contact) modulus, the impact velocity, and the reduced radius of curvature ($1/R = 1/R_1 + 1/R_2$), respectively. The dynamic hardness can be related to the more commonly well-known static hardness of the material through a material-specific factor, as shown in the works of Tabor [40, 43]. As can be seen, e varies with $v_{imp}^{-1/4}$ [42], demonstrating the trend of decreasing COR for increased impact velocity:

$$e = 1.88 \left(\frac{p_d}{E^*}\right)^{\frac{1}{2}} \left(\frac{\frac{1}{2} m_s v_{imp}^2}{p_d R^3} \right)^{-\frac{1}{8}} \tag{12.5}$$

There are many other collision situations such as repeated impacts [44], spheres colliding with thin plates (as compared to sphere diameter) [36, 45–47], sphere–sphere collisions [48–50], oblique impacts [51–53], and the collision of spheres and boundaries in fluids. Gondret et al. [54], Joseph et al. [55], and Ruiz-Angulo and Hunt [56] have studied the COR for these fluid-based collisions extensively. However, this work goes beyond the scope of the current section on dry granular flows.

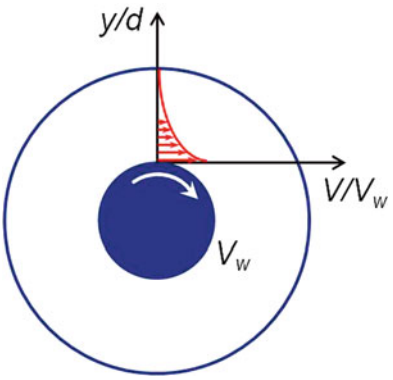

Fig. 12.4 Schematic of an annular geometry with a velocity profile (adapted from MiDi [61])

2.2.2 Granular Flow Experiments

The previous section detailed experiments performed at the local (single-particle) level, namely, COR. At the global (bulk) flow level, a number of experimental studies have been performed to gain insight into the behavior of granular flows inside of tribosystems, such as those seen in Fig. 12.1. As such, this section focuses specifically on experimental work performed using the annular, parallel, and converging geometries shown in Fig. 12.1. These tribologically relevant sliding contact geometries are discussed in detail, with their examination being adapted from the work of Wornyoh et al. [4]. Other common, but less (non-)tribologically relevant, granular flow geometries are briefly highlighted at the end of the section.

Annular geometry refers to the concentric cylinder setup shown in Fig. 12.1a, where the granular flow resides in the annular gap between the cylinders which slide relative to one another. The pioneering experiments of Bagnold [57] were the first to study the flow of granules under shear. He sheared a dispersion of uniform-sized, solid spherical grains in Newtonian fluid in annular space between two concentric drums. Two distinct regions, grain–inertia region and macroviscous region, were identified, and empirical relations for shear stress were formulated. He also established a third transition region. Representative results for a number of granular experiments [58–60] performed using the annular geometry can be found in the detailed review of MiDi [61]. MiDi [61] summarized experiments and simulations conducted on dense (high solid fraction) granular flows and classified them into six geometric configurations. Figure 12.4 (adapted from MiDi [61]) shows a schematic of the annular flow geometry and velocity profile. In Fig. 12.4, the velocity profile displays an exponential decrease in velocity when moving from the inner rotating wheel to the outer stationary wheel (cylinder). This is typical of many experimental velocity profiles, as detailed in MiDi [61]. It is also shown that for annular geometries, volume fraction shows a slight increase when moving away from the inner wall, while velocity fluctuations (when plotted on a log scale) show a relatively linear decrease when moving across the annular gap [61].

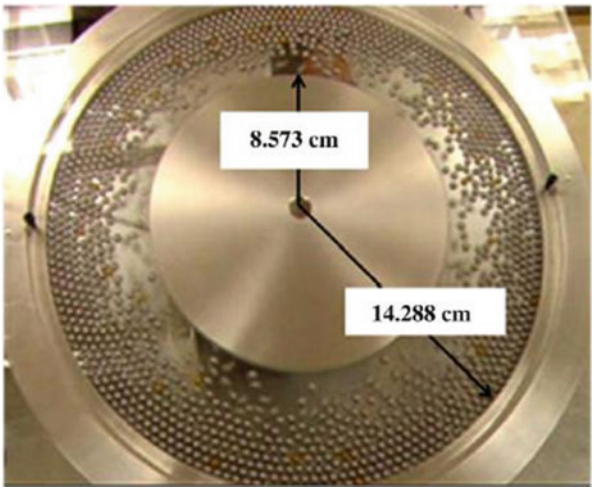

Fig. 12.5 Granular shear cell (GSC) [35]

Other annular-type experiments include the work of Tardos et al. [62] which sheared a bed of fine glass beads between concentric rough vertical cylinders and measured the shear and normal stresses. Veje et al. [63] sheared photoelastic disks at slow rates in a two-dimensional annular setup with a rough rotating inner wheel. Velocity, spin, and solid fraction distributions were measured by means of digital particle tracking. Howell et al. [64] used the same annular setup as Veje et al. [63] to measure the stress fluctuations using photoelasticity. Mueth et al. [59] combined three noninvasive techniques—magnetic resonance imaging (MRI), x-ray tomography, and high-speed-video particle tracking—to obtain the particle velocity, spin, and solid fraction data in three dimensions. They sheared mustard and poppy seeds between concentric rough cylinders. Losert et al. [65] sheared black glass beads between a rotating inner cylinder and outer cylindrical frame. Mean particle velocities and velocity fluctuations were measured as a function of distance from the rotating wall [65]. The inner and the outer cylinder walls were coated with glass beads to make them rough. These experimental results [65] were compared to a continuum model developed by the same researchers in the work of Bocquet et al. [60].

Higgs et al. [10], Jasti and Higgs [66], and Marinack et al. [35] made use of the granular shear cell (GSC) shown in Fig. 12.5 to study granular material in an annular configuration (Fig. 12.1a). The GSC is unique in that it provides a variable and quantifiable macroscopic roughness on its inner driving wheel as shown in Fig. 12.6. These works [10, 35, 66] obtained data for the granular velocity, solid fraction, granular temperature, and slip velocity by averaging discrete particle data gathered in radial bins. Representative results from the GSC [35] are shown in Fig. 12.7 for granular velocity, solid fraction, and granular temperature. Slip velocity at the boundary of the inner wheel can also be obtained as the difference between the wheel's linear surface velocity and the velocity of the granules in the bin adjacent to the inner rotating wheel.

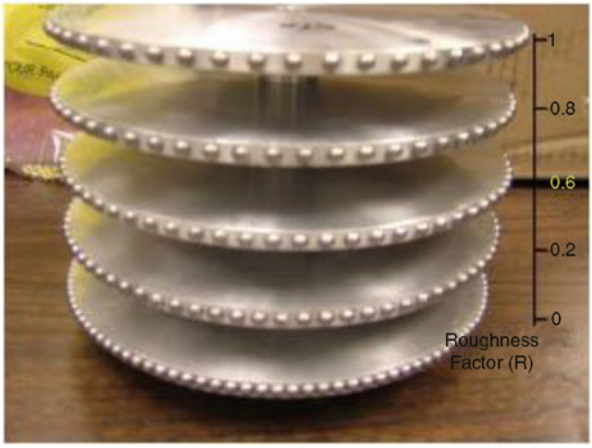

Fig. 12.6 Macroscopic roughness factor on the GSC in the form of granules glued at fixed distances along the wheel's outer edge [66]

Figure 12.7a displays one of the interesting behaviors from these experiments [35, 66], which is the development of two distinct regions inside the flow. The region near the inner rotating wheel is termed the kinetic region, where the flow is sparsely populated, and characterized by high-speed collisions with short contact times. In these types of collisions, extended sliding between granules, in which frictional effects become more significant, is unlikely. As a result, the coefficient of friction (COF) between colliding particles tends to have a much smaller influence on the flow characteristics than does the coefficient of restitution (COR). In contrast, the contact region (region adjacent to the outer wall) is densely populated and depicted by extended frictional (sliding) contacts. This leads to the COF, as opposed to the COR, being more influential on the characteristics and properties of the contact region [35].

The tangential velocity profile in Fig. 12.7b shows a decrease in velocity when moving from the inner wheel to the outer rim. A distinct transition between the two regions (regimes) is witnessed, where velocities in the contact region approach zero. The velocity profile (Fig. 12.7b) also displays a significant amount of slip at the driving (wheel) surface, which is a common difference between granular and traditional fluid flows. The solid fraction is a minimum near the wheel (Fig. 12.7c) and increases while moving outward to the contact region. The granular temperature (Fig. 12.7d) follows a similar trend as the velocity (Fig. 12.7b).

Parallel geometry (see Fig. 12.1b), often called "parallel type," refers to horizontal plates or "racetrack" geometries, which are commonly studied for first-order predictions and as idealistic conditions. Savage and Sayed [67] developed and performed experiments on annular shear cells with various granular materials, at rapid shear rates. Though the setup was annular, the shear zone was parallel type. They determined the effects of shear rates and solid fraction on shear and normal stresses. Similar to the annular shear cell, a parallel-plate shear cell was used to shear glass spheres mixed with water or air at high speeds by Hanes and Inman [68]. They observed two types of flows. At high shear rates, all the granules in the

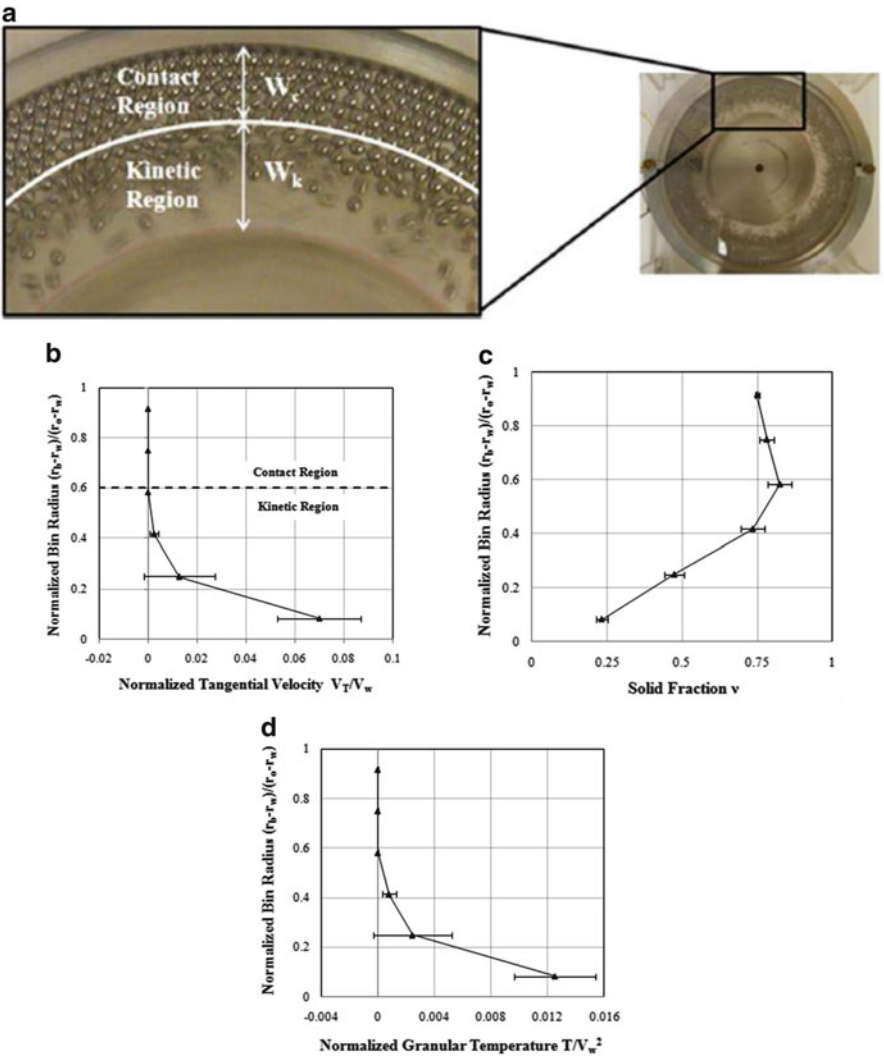

Fig. 12.7 Experimental results for the granular shear cell (GSC) [35]: (**a**) image of experiment displaying kinetic and contact flow regions, (**b**) velocity profile, (**c**) solid fraction profile, and (**d**) granular temperature profile

shearing gap were mobile. On the other hand, in the second type of flow, some granules remained stationary and others were sheared rapidly creating an internal boundary.

Miller et al. [69] performed experiments on variable-sized glass beads by shearing them in a Couette parallel geometry. They measured the fluctuations in normal stress. Yu et al. [2] sheared glass beads in a parallel shear cell apparatus in order to measure normal and shear stresses. This is the first experimental work that refers to

normal stress as load and shear stress as a frictional stress. They also proposed the idea of granular kinetic lubrication in this paper. Effects of surface roughness, particle size, and solid fraction are further elaborated using the same setup as Craig et al. [70, 71]. Elkholy and Khonsari [3] performed experiments to investigate the characteristics of granular collision lubrication by using a rig similar to that of Yu et al. [2]. In their work [3], three regions were witnessed along the width of the flow. The first region consisted of the granules adjacent to the upper moving wall; the second was the "locked" (or jammed) granules adjacent to the bottom stationary wall; and the third region was the transitional region in between [3].

Converging-type geometry, also called bearing type, usually refers to a geometry that has a converging region that the particulate materials are entrained in during operation to produce a lubrication effect, as seen in Fig. 12.1c. The shear cell apparatus developed by Yu et al. [2] was adjustable such that it could have a flat shear surface or a surface containing three sloping regions with a step. This geometry created a converging gap between shearing surfaces. They confirmed that lubrication wedge effect exists and that the (lubrication) normal stress is roughly proportional to the square of the surface slope. Additional experimental studies into converging gap geometries can be seen in the experimental investigations into the behavior of planetary rover wheel–terrain interactions, which have already been mentioned and discussed in Sect. 2.1.

2.3 Modeling

Granular flow modeling can be divided into two categories or factions. These categories are discrete and continuum modeling. Discrete modeling treats each individual particle within the flow as a single entity while discretizing time into individual time steps at which the particles can move and interact with each other and the boundaries. In a discrete modeling approach, all the granules are tracked at every time step and simulations are driven by the collisions and interactions of the individual granules. Flow parameter results are obtained by means of averaging discrete particle data from the individual granules in the flow. In contrast, continuum modeling treats the granular flow as a fluid-like continuum through the use of mass, momentum, and energy conservation equations, with granular modifications, to describe the flow. These conservation equations can be paired with constitutive relations and boundary and initial conditions to effectively solve for the flow parameters of interest, in the same manner that the Navier–Stokes equations might be solved for a fluid. This section will discuss the three main discrete modeling approaches as well as continuum modeling.

2.3.1 Discrete Modeling

There are three major discrete modeling approaches which will be discussed in this section. These three approaches include the discrete element method (DEM),

lattice-based cellular automata (CA), and the explicit finite element method (FEM). As will be detailed in the following sections, these discrete approaches differ in significant ways such as their particle physics, spatial discretization, and/or processing algorithms.

Discrete Element Method (DEM)

The discrete element method (DEM) of particle modeling, originally introduced by Cundall and Strack [72], treats each particle as an individual and singular entity which moves freely through space (at fixed time intervals), participating in interactions with other particles and boundaries. DEM modeling can be split into two main classifications: the hard-sphere (body) model and the soft-sphere (body) model.

Hard-Sphere DEM: The hard-body model assumes that particle collisions are instantaneous, nonoverlapping, and binary, meaning that one particle may only interact with one other particle in a given time step. As a result of not having to incorporate multi-particle contacts, the hard-body model can utilize a larger time step and is better suited for dilute flows. Particle collisions are generally solved through the use of coefficient of restitution (COR), coefficient of friction (COF), and coefficient of rotational (tangential) restitution (CORR) interaction parameters. Walton [73] provides a friction-inclusive hard-sphere collision model which is essentially an extension of the works of Hawkins [74] or Hopkins and Shen [75]. This model [73] serves as a good representation of collision processing within hard-sphere collision models and is thus presented in detail. The hard-sphere model presented in Walton [73] is based on the use of the three previously mentioned parameters: COR (e), COF (μ), and CORR (β_0). Conserving linear momentum and making use of the definitions of the coefficient of restitution ($e = v'_n/v_n$) and the coefficient of rotational restitution ($\beta = -v'_s/v_s$) result in (12.6) and (12.7) for the changes in normal direction velocities (Δv_{na} and Δv_{nb}) of two colliding spheres (denoted a and b):

$$\Delta \vec{v}_{na} = \frac{m_b(1+e)}{m_a + m_b} \vec{v}_n \tag{12.6}$$

$$\Delta \vec{v}_{nb} = \frac{-m_a(1+e)}{m_a + m_b} \vec{v}_n \tag{12.7}$$

where m and v_n represent the mass of the particles and the relative normal velocity, respectively.

In terms of application of the hard-sphere model, Campbell and Brennen [76] compared their two-dimensional simulations of collisional granular flows to experiments by Savage and Sayed [67] and Bagnold [57]. Hopkins and Louge [77] developed a two-dimensional computer simulation for rapidly shearing uniform smooth inelastic disks. They compared the results to the theoretical

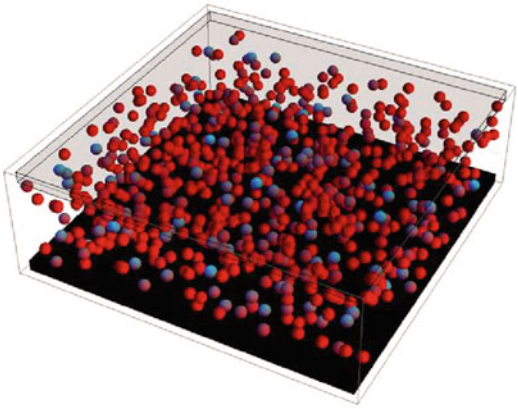

Fig. 12.8 Couette shear cell simulation domain (similar to that of Louge [81])

model of Jenkins and Richman [78] with good agreement. Sawyer and Tichy [79] performed numerical and particle dynamic simulations to generate results that were compared to the granular experiments of Yu and Tichy [80]. Louge [81] examined the interaction of a rapid granular flow with a flat, frictional wall, by means of a simulation domain similar to the one shown in Fig. 12.8, with the addition of hemispheres along the upper wall. In this same work, Louge [81] also displays results for the dynamic friction coefficient vs. normalized slip at the wall at varying friction coefficients. Louge [81] compares numerical simulation results against theoretical predictions from Jenkins [82].

Soft-Sphere DEM: In contrast to the hard-body approach, the soft-body particle collision model treats the granules as deformable spheres which allows for enduring (over multiple time steps) and multiple particle contacts. This requires the soft-body approach to employ a relatively small time step. In the soft-body collision approach, particle interactions are governed by force laws which determine the sum of the forces acting on the particles and hence dictate the resultant motion of the interacting particles. As a result, the soft-body approach is well suited for modeling dense granular flows where multi-body contact is prevalent.

Examples of force models and equations used in the soft-body modeling approach are provided by McCarthy et al. [83]. This set of force models (equations) is presented as merely a sampling of the types of equation used in the soft-body approach. There are certainly a wide range of other force equations and models available. In terms of normal forces, two separate force models are examined. The first normal force (F_n) model is a spring–dashpot model shown in (12.8):

$$F_n = k_n \alpha^{3/2} - \beta \alpha \dot{\alpha} \tag{12.8}$$

The first term acts as the "spring" term, where α and k_n represent the particle overlap and the normal force constant from Hertz theory [42], respectively. The second term acts as the "dashpot," where β and $\dot{\alpha}$ define the damping parameter and the relative normal velocity of the colliding particles, respectively. A plastic normal

force model is also examined in the work of McCarthy et al. [83] and is shown in (12.9):

$$F_n = F_y + k_y\left(\alpha - \alpha_y\right) \tag{12.9}$$

The variables F_y and k_y respectively define the yield force and plastic stiffness ($k_y = (3/2)(F_y/\alpha_y)$). The variable α_y is the deformation at the point of yield. A tangential force (F_t) model is shown in (12.10):

$$F_t = F_{t_0} - k_t \Delta s \tag{12.10}$$

In (12.10), F_{t_0}, k_t, and Δs define the initial tangential force during the previous time step, the tangential stiffness, and the tangential displacement during the current time step. The quantity $k_t \Delta s$ gives the incremental change in tangential force during the current time step based on relative particle motion. Finally, a rolling friction model is also included, where the torque resisting the rolling motion (M_r) is calculated as shown in (12.11):

$$M_r = -\frac{3\gamma}{16} a F_n \frac{\omega}{|\omega|} \tag{12.11}$$

In (12.11), γ, a, and, ω define the fraction of energy lost in a single rotation, the radius of the contact spot, and the angular velocity of the particle, respectively. By defining a coefficient of rolling friction as $\mu = 3\gamma a/16R$, this (12.11) can be reduced to (12.12):

$$M_r = -\mu_r R F_n \frac{\omega}{|\omega|} \tag{12.12}$$

Overall, the discrete element method provides for a large amount of accuracy in the simulation of granular flows. The development and use of numerous force and particle interaction models allows for rigorous modeling of granule interactions at the local level. This results in DEM being able to provide good quantitative and qualitative predictions for a number of flow situations. As a result, DEM is often considered the "gold standard" in granular flow modeling. The one major drawback of the discrete element method is its computational cost. As a result of its rigorous modeling, DEM simulations tend to be extremely computationally demanding and costly. This becomes particularly concerning as the number of particles being simulated is increased.

Cellular Automata (CA)

Cellular automata (CA), originally introduced by von Neumann [84] in his study of biological systems, is a discrete modeling platform for obtaining fast first-order

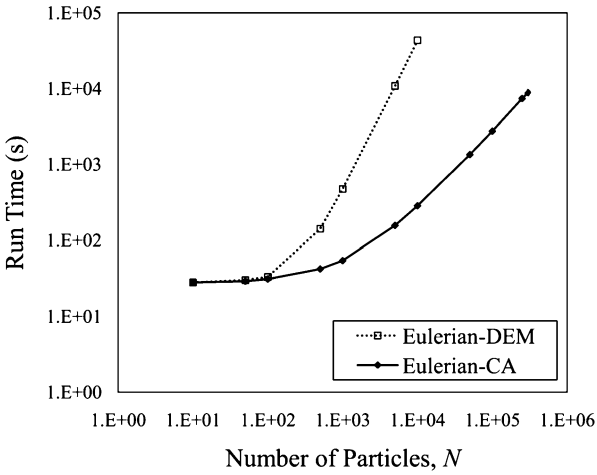

Fig. 12.9 Time study for CA vs. DEM at increasing particle counts, as presented in Marinack et al. [86]

approximations of the properties of many physical systems, such as local granular flow properties. CA modeling uses either rule-based mathematics or physics-based equations to model physical processes (such as granular flow). It does this on a lattice, where space is divided into cells and each cell exists in one of a defined number of states.

CA is based on several fundamental principles, which are common among CA modeled systems. These principles, outlined in Ilachinski [85], include:

1. Space is represented by a uniform grid made up of discrete cells.
2. Each cell should be in one of a finite number of fixed states.
3. Cells may change states only at fixed, regular intervals of time.
4. States are updated in accordance with fixed local rules operated on an interaction neighborhood.

The major advantage of using a CA model is its computational efficiency. For example, a multiphase (solid particle–fluid) flow model, which combined computational fluid dynamics to model the fluid phase and CA to model the particle phase [86], has demonstrated the potential computational advantages of using a CA approach over DEM. It did so by comparing the CA model's run times for simulating ten real-time seconds of a low solid fraction multiphase flow between parallel plates against run times for a model using DEM for the particle phase. As shown in Fig. 12.9, as the number of particles in the simulation domain increased, CA provided for an increasingly large amount of time savings. Another advantage of the CA model is that because the particles are on a lattice and only move based on neighbor interactions, no particle interaction behavior is missed. Additionally, the spatial lattice is inherently comprised of neighborhoods, which can each be processed in parallel.

The disadvantages of the CA model include an accuracy trade-off and some simulation limitations. While CA is a fast first-order modeling approach, the computational efficiency of CA leads to a trade-off in accuracy as compared to

the DEM approach. Additionally, the lattice-based spatial discretization scheme makes it impossible to model length scales smaller than the size of a lattice cell. Additional comments and details on the strengths and limitations of a CA framework are given by Jasti and Higgs [87].

CA has been used to model a wide array of granular behavior, including segregation [88–90], heap formation [91–93], and flow down silos and hoppers [94, 95]. Particle interactions in a CA model can be derived from empirically based rules (often from lookup tables), rule-based mathematics, or physics-based equations. The Higgs' group began employing physics-based particle interaction equations to granular tribology problems through the CA modeling framework [87, 96]. Other works [89, 91, 93, 94] consider the dissipative nature of COR and COF in processing particle interactions. However, they do not apply them directly through the solving of physics conservation equations, but rather through rules based on probability.

Jasti and Higgs [97] applied a CA modeling approach to granular flow lubrication and compared results from the CA simulations to the granular kinetic lubrication (GKL) model [1]. The GKL model is a continuum approach that applies rheological constitutive equations for stress, conduction and dissipation to thin granular shear flows, as well as rigorous boundary conditions for momentum and energy transport [1]. Particles in the CA model from Jasti and Higgs [97] were processed primarily with a rule-based approach as shown in Fig. 12.10. Figure 12.10 displays the rules for processing particle–particle interactions inside of the parallel-type shear cell geometry. The results from the CA simulations were promising as they showed a favorable match to results from the GKL continuum model [1] for the prediction of slip at the wall of a shear cell. Other uses of CA in granular tribology include Osterle et al. [98], who used a CA modeling approach to examine the flow of third bodies during dry sliding in automotive braking technology.

Jasti and Higgs [87] applied CA modeling to annular-type geometries (see Fig. 12.1a), namely, the granular shear cell (see Fig. 12.5). Marinack and Higgs [96] extended this CA framework to include interparticle friction and spin. In this work [96], particles which collided on the CA grid were processed using the full model from Walton [73], as presented previously during the discussion of hard-sphere DEM. The simulation representation of the GSC and velocity profile results from this work [96] are shown in Fig. 12.11. For relatively dilute flows (see Fig. 12.11a), results showed that the CA model which accounted for friction compared much more favorably to the experiment than the frictionless CA model.

Finite Element Method (FEM)

The finite element method (FEM) has become widely used in the tribology community to study complex contact, thermal, fluid, and structural interaction. In the finite element analysis arena, two distinct methods, the implicit and explicit time integration techniques, have emerged for simulating engineering and scientific problems. Although both of these methods are used to solve the same basic set of

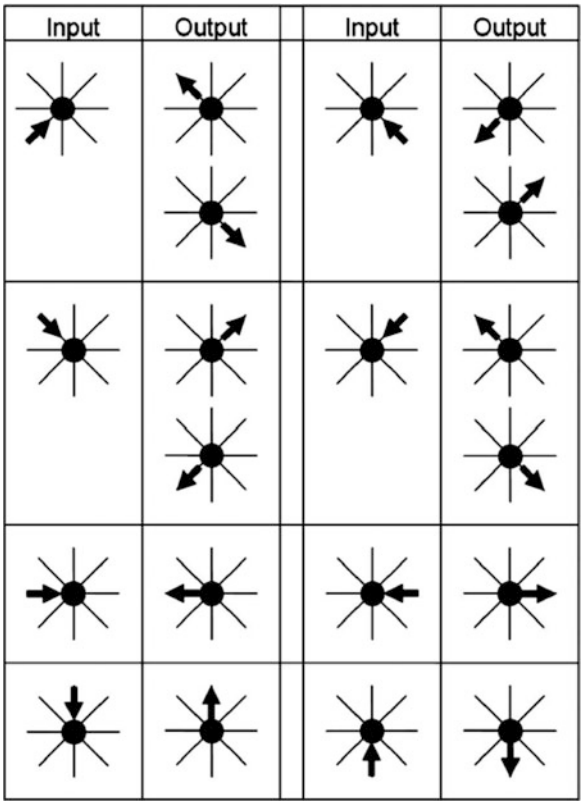

Fig. 12.10 Rules for processing particle–particle interactions in the model of Jasti and Higgs [97]

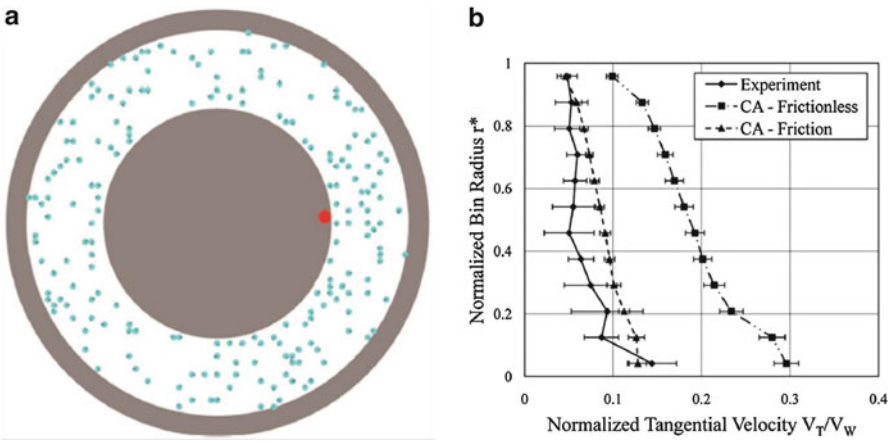

Fig. 12.11 CA simulation of the GSC (Fig. 12.7) from Marinack et al. [96]. (**a**) The simulation domain. (**b**) Velocity profile results for experiment and CA simulation

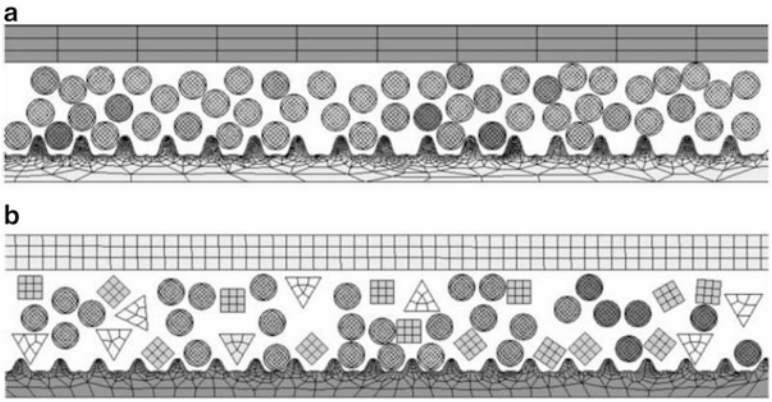

Fig. 12.12 Meshed finite element models [100] with (**a**) round particles and (**b**) multi-shaped particles

governing equations, the primary applications for which each method obtains a robust accurate solution are vastly different. Explicit FEM was originally developed to solve problems in wave propagation and impact engineering, but more recently, it has been applied to diverse areas that include sheet metal forming, underwater simulations, failure analyses, glass forming, metal cutting, pavement design, and earthquake engineering [99]. Since the method is good for highly transient events, the explicit FEM approach has been employed in granular flow tribology.

Kabir et al. [100, 101] first introduced the explicit FEM approach for granular modeling. In these works [100, 101], the explicit FEM method (using LS-DYNA software) was applied to modeling parallel (Couette) shear cells where the top wall remained stationary while the rough bottom wall moved at a fixed velocity. Figure 12.12 shows examples of two meshed finite element models [100], one of which contains round particles (Fig. 12.12a), while the other contains multi-shaped particles (Fig. 12.12b). In both cases, the roughness bumps on the bottom wall can be seen. As can be seen in Fig. 12.12, the particles themselves are meshed and thus comprised of a number of elements. This is in contrast to the previously examined discrete element method (DEM) and cellular automata (CA) approaches, which treat each particle as a single entity. As a result of individual particle meshing, the stress distributions inside of the particles can be obtained. This ability allows for many interesting phenomena to be witnessed in explicit FEM simulations, such as the breaking and forming of force chains. Figure 12.13 [100] displays an example of this behavior where a chain of particles spans the gap from the upper to lower wall. The stress distribution is easily viewed, obviating the formation of a force chain throughout these particles.

There are several advantages that make FEM uniquely suited to model granular flow tribosystems. First, FEM allows deformations of the grains to happen in silico (i.e., during the simulation), which means that the surrounding particles have to

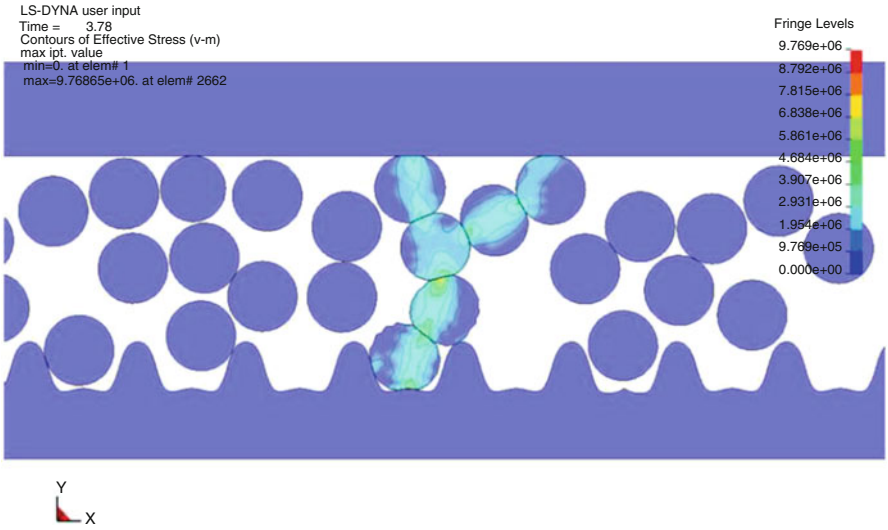

Fig. 12.13 Stress and deformation plot from an explicit FEM study of a shear cell, performed in the work of Kabir et al. [100]

react to a newly deformed geometry, where particles have modified shapes and contact behavior. Secondly, the explicit FEM approach can handle complex boundaries and aspherical particles (as shown in Fig. 12.12b), since the FEM framework meshes all solid objects with a finite set of elements that can be assigned varying material behavior. This also enables FEM to accommodate heterogeneous materials with varying mechanical properties or material behavior. Third, the main material information needed to simulate the contact and collision behavior of grain flow is the mechanical properties, since the FEM framework is fundamentally solving the continuum equations of solid mechanics. Thus, collisional system parameters such as the coefficient of restitution can be predicted in FEM whereas it is normally required as input in the DEM and CA approaches. As such, FEM work to predict COR has been done to consider elastic and elastic–plastic impact of spheres against substrates of varied thickness [102], repeated impacts [44], and many other collision situations [49, 103–105]. There are two major disadvantages of the explicit FEM approach with application to discrete grain simulations. First, as it is not an implicit approach (i.e., unconditionally stable for large time steps), smaller time steps have to be used to maintain stability. The time step in the explicit FEM approach must not exceed $\Delta t = L_e/c$, where L_e is a mesh element length and c is the wave propagation velocity through the material [106], which is often the speed of sound. Therefore, the time step scales down with increased FEM mesh resolution. Second, as the FEM particles are meshed (as opposed to a single element per particle in DEM or CA), computational costs per contact event are higher than the mesh-free particles.

2.3.2 Continuum Modeling

This section is adapted from the detailed review performed by Wornyoh et al. [4]. Since granular flows exhibit fluid-like behavior, continuum approaches for modeling granular flows have used the conservation equations for mass, momentum, and granular energy, which take into account velocity fluctuations and the inelastic collisions of particles. Once obtained, the governing equations are solved for parameters such as velocity, solid fraction (or density), friction coefficient, and load-carrying capacity. Constitutive relations are also needed to describe the behavior of dry particulates, in addition to describing the behavior of the particulates at the surface boundaries.

The granular tribology community [1, 79, 107, 108] has employed granular forms of the conservation equations as described by either Haff [109] or Lun et al. [110]. The conservation of mass equation for granular flows is of the form

$$\frac{D\rho}{Dt} = -\rho\left(\vec{\nabla}\cdot\vec{U}\right) \tag{12.13}$$

where the granular flow density ρ and granular mixture velocity U are the key parameters. The granular conservation of momentum equation is

$$\rho\frac{D\vec{U}}{Dt} = \rho\vec{g} - \nabla\cdot\vec{\pi} \tag{12.14}$$

where $\vec{\pi}$ is the stress tensor and $\vec{g}$ is the body force vector. The granular conservation of energy equation is also known as the pseudoenergy equation. It is similar to the conventional energy equation for fluids except that the rate of change of the granular temperature is balanced against the energy added and dissipated from the system due to friction and inelastic particle collisions. The granular temperature is a measure of the fluctuating component of the granular particles relative to the mean granular velocity field [111]. Thus, it is written as

$$\frac{3}{2}\frac{D(\rho T)}{Dt} = -\vec{\nabla}\cdot\vec{q} - \varphi^f - \varphi^c \tag{12.15}$$

where $\vec{q}$ is the molecular energy transport, φ^f is the work rate of momentum, and φ^c is the inelastic work rate (dissipation due to inelastic particle collisions). Details on (12.13)–(12.15) can be found in Higgs and Tichy [1].

Haff's continuum theory and constitutive relations [109] for describing the motion of granular material are used frequently by granular tribologists ever since Elrod took the "first look" in his granular tribology review paper [112], which focused largely on granular flows. Adopting Haff's constitutive relations, Dai et al. [113] worked to determine the capability of granular flows to be viable mechanisms for lubrication in slider bearings. Subsequently, McKeague and

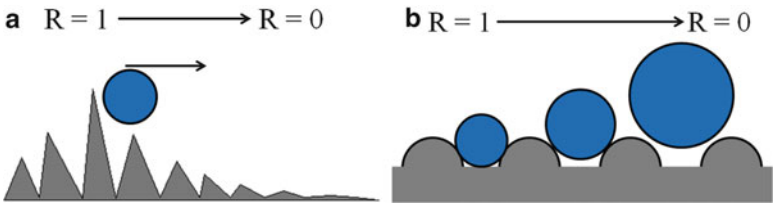

Fig. 12.14 Roughness factor schematic (adapted from [4]). The roughness factors are defined as: (**a**) the fraction of lateral momentum imparted to the granule by the surface and (**b**) the fraction of a granular particle that fits between wall hemispheres

Khonsari [5] used his theories to perform parametric studies with granular flows and also to predict the hydrodynamic pressure profiles from the well-known powder lubrication experiments of Heshmat [114]. Tribologists have also used constitutive relations by Lun et al. [110] to model granular flows in parallel sliding contacts under load [1, 79, 108, 110] and granular slider bearings [115].

Developing relations to describe the behavior of granular materials around the boundaries is also important. The boundary equations in the granular tribology community are often derived from the work of Jenkins and Richman [116] and Hui et al. [117]. In these works, the macroscopic roughness factor R varies as $0 \leq R \leq 1$, where $R = 0$ corresponds to a fairly (macroscopically) smooth surface and $R = 1$ corresponds to a very (macroscopically) rough surface. It has been characterized in Fig. 12.14 as the fraction of lateral momentum transferred to the granular flow by the walls [118] and the fraction of a granule that fits exactly between the cylindrical wall disks [119]. The roughness factor affects the slip at the boundary, which ultimately affects the granular film's ability to accommodate velocity and carry load.

3 Slurry Tribology

"Slurry tribology" is the study of particle–fluid suspensions as they relate to friction, lubrication, and wear. In tribology, slurries are often used to remove materials from surfaces in a controlled manner [120–123]. However, oftentimes, engineering solutions are sought to reduce the amount of material removed from surfaces due to slurry wear mechanisms such as abrasion and erosion [124]. In other scenarios, slurries formed by adding lubricious particulates to fluid lubricants can actually increase bearing life [125]. Though the behavior of a slurry in a tribological environment is complex, many people are already familiar with natural processes that are dominated by slurry tribology. The erosion of riverbeds due to small rocks suspended in the flow is also a slurry tribological phenomenon.

In one of their most familiar tribological applications, slurries are used as lapping and polishing compounds for the preparation of test specimen surfaces. The micron- and submicron-sized particles used in these polishing applications are

essential for achieving the desired surface finishes. Though there are many different particle types in slurries, a few of the most common ones used in slurry polishing are silica, alumina, and synthetic diamond. The specific abrasive particle type is chosen based upon parameters such as the material being polished, the base fluid in which the particles are suspended, the polishing load and speed, and the desired surface finish. Typically, the smaller the particle size, the better the surface finish (i.e., lower surface roughness) as large particles may remove more material and produce unwanted scratches. This type of slurry polishing has been used for years with much success. Currently, there are many new and exciting applications of slurry tribology.

3.1 Slurry Tribology Applications

In this section, three important uses of slurry tribology in relation to nanofabrication, lubrication, and energy production are discussed.

3.1.1 Slurry Tribology in Nanofabrication

Over the last several decades, chemical mechanical polishing (CMP) has become a fundamental application of slurry tribology [126]. CMP is used to fabricate computer chips or integrated circuits (ICs) because of its ability to planarize and polish the large wafers on which ICs are built. During CMP, the wafer is pressed into a soft rotating polishing pad. Between the pad and the wafer, a chemically-active slurry, containing abrasive nanoparticles, is entrained. Though there is still discussion in the literature regarding the details of the wear mechanisms in CMP, it is generally accepted that the nanoparticles in the slurry abrade the wafer to remove unwanted material from its surface. In Fig. 12.15, an image of the G&P Poli-300 CMP machine is displayed.

Though widely used in the IC fabrication industry, improper CMP is known to impart defects on the IC's [122]. As the IC is built, nano-sized trenches are etched into the dielectric materials (mostly silicon dioxide) on the surface of the wafer. Conductive copper is deposited into these trenches to form copper lines which serve as the wires in the IC. To ensure that the trenches are filled, it is easier to deposit copper over the entire wafer and remove the excess using CMP. Once much of the excess copper has been removed, the resulting wafer surface is a heterogeneous combination of soft copper and hard dielectric materials. The difference in material properties between the copper and the dielectric can result in differential wear rates as CMP is performed. Two defects which occur during this CMP process are commonly known as "dishing," which is unwanted material removal from the copper line, and "erosion," which is unwanted material removal of the dielectric. Moreover, contact stresses and fluid pressures in the slurry can cause changes in material removal rates at the edge of the wafer. This unwanted material removal can

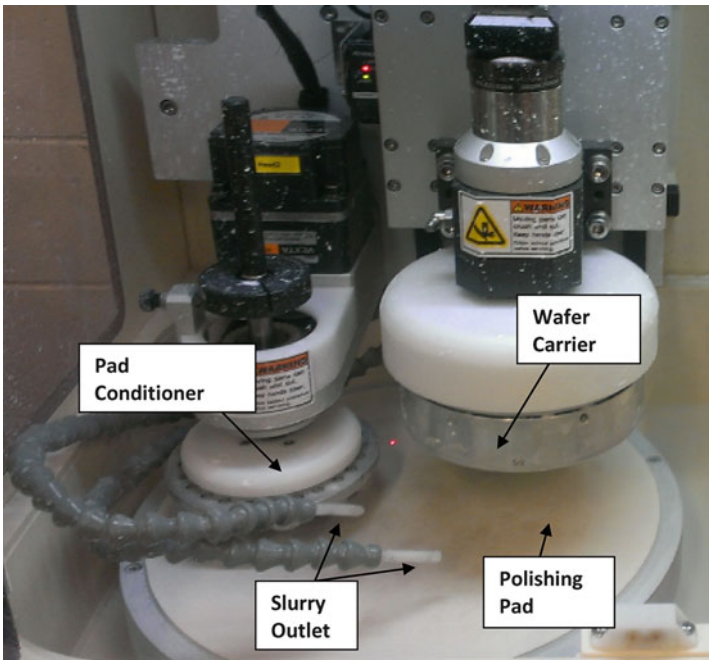

Fig. 12.15 An image of the G&P Poli-300 CMP machine

result in electrical shorts or open circuits which may ultimately require the IC to be discarded. Understanding the mechanics of the slurry during CMP can lead to a reduction of such defects [126].

3.1.2 Slurry Tribology in Lubrication

Greases and oils provide essential lubricant films for machine components such as bearings, gears, chains, and seals. However, when tiny particulate matter is entrained into these lubricants, a slurry is formed which, in many cases, exacerbates wear and reduces the lifetime of the hardware [127]. Once the particles get into the interfacial film, they can disrupt the load-carrying capacity of the film and reduce the lubricant's effectiveness. If the particles are so large that they transmit load between the surfaces, stresses on the surfaces can result in unwanted wear.

There are several examples of this phenomenon. In the internal combustion engine, the air filter helps to prevent particulate matter from entering the engine. However, when sand or dirt particles in the air intake make it past the air filter, these particles can enter the combustion cylinder and make their way into the lubricant system. Notably, they can become trapped in the lubricant film on the piston rings and cause abrasive wear damage to the cylinder walls [127]. In internal combustion

engines, particulates are also generated as a result of the combustion process itself. Soot particles can be formed which affect the lubricant's performance. Finally, a third example is the generation of particulate matter due to wear debris. During startup and shutdown, bearings are particularly vulnerable to wear as they transition into the mixed and boundary lubrication regimes. Once this happens, wear debris can be introduced into the lubrication system. Oil filters in engines are used to help remove particulate debris from the lubricant to minimize the effect of these wear particles.

Artificial Joints

Another example of slurry formation in lubricants occurs in the human body. When hip and knee replacements are performed, cements, such as polymethyl methacrylate (PMMA), are used to bind materials together. Over time, the PMMA can chip generating sharp fragments which make their way into the synovial fluid forming a slurry. This slurry of synovial fluid and PMMA fragments can be detrimental to joints and cause unwanted wear to them [128].

Particle Additives

It should be noted that not all slurries are detrimental to lubricated interfaces. Particle additives such as polytetrafluoroethylene (PTFE) and molybdenum disulfide (MoS_2) have been discussed in the literature for years. Some studies indicate that the effect of such additives may increase bearing performance [129] and this practice has been adopted commercially. There is, however, a balance between particulate additives acting to increase the bearing performance and the potential for them to clog the interface reducing the entrainment of lubricant into the bearing. That has led to the emerging and exciting new field of nano-fluid slurry lubricants. Nano-fluid slurry lubricants are fluid lubricants to which nanoparticles have been added. The particles in nano-fluid slurries may be large enough to help lubricate the interface during boundary and mixed lubrication but small enough to reduce the potential for clogging [125, 130]. Additionally, because of their fine size, nanoparticles may form a more uniform protective layer on the surfaces as compared to larger micron-sized particle [131].

There have been several studies which have investigated the use of nanoparticles as lubricant additives which show great promise in improving bearing performance. In a recent work, boric acid particles were added to environmentally-friendly lubricants, such as canola oil, and displayed a reduction in friction [130].

As a final example of the potential benefits of particles in lubricants, there is a class of bearings called "two-phase porous" bearings which rely on the presence of particles, advected by the lubricant, to clog pores in the bearing surfaces reducing their porosity. Once the porosity of the bearing is reduced, sufficient film pressures are generated to carry the bearing loads [132].

3.1.3 Slurry Tribology in Energy Production

Slurry tribology is an important component in energy production. There are several examples of the role of slurry tribology in the petroleum industry. Petroleum and natural gas reserves are found deep under the Earth's surface. When drilling for these fuel reserves, it is common to use a slurry to lubricate the drill bit as it cuts into the rock formation [133]. This slurry, called a drilling fluid (often referred to as a drilling "mud" in the field), is an important component in the drilling process. The drilling fluid (1) lubricates the drill bit, (2) removes heat from the rock–drill bit interface, (3) transports rock cuttings away from the well bore, and (4) helps to prevent well blowouts by keeping formation fluids from prematurely entering the well bore.

Typically, the drilling fluid slurry is either oil based or water based and contains particles such as calcium carbonate. By adjusting the concentration of particles and the particle type, the drill operator or "mud engineer" responsible for the drilling fluid can "tune" the drilling fluid's properties to better perform its tasks.

A closely related application of slurry tribology is a process called hydraulic fracturing. During hydraulic fracturing (often called "fracking"), fracturing fluid is pumped into fissures and cracks in the rock formation. The high pressure of the fracturing fluid fractures the rock formation releasing pockets of trapped gas. Much like drilling fluid slurries, fracturing fluid slurries are comprised of a base fluid and loaded with particulates to enhance their performance.

Finally, after the petroleum fluids have been taken from the ground, sand and dirt in raw petroleum fluids create a slurry which can cause erosive wear to pipe surfaces as it is being transported long distances to refineries. This erosion is particularly severe at areas where the fluid changes directions or velocities sharply such as pipe elbows, tees, and valves [124].

3.2 Slurry Tribology Experiments

Before using a slurry in tribological applications, it is important to test its performance. There are many devices that have been created which can assess the performance of slurries. One such device is a multipurpose tribometer. These types of instruments can be configured to conduct experiments such as pin-on-disk tests in which a slurry can be introduced into the interface. Additionally, some of the machines can be configured to do benchtop CMP to test the performance of different CMP slurries. Moreover, 4-ball tests can be run with contaminated lubricants to test their effect on potential ball-bearing applications. In Fig. 12.16, an image of the CETR UMT multipurpose tribometer is displayed.

In addition to these multipurpose slurry tribometers, there are also a host of highly specialized tribometers which are used to test slurries in extreme conditions using specialized materials. An example of this is the spiral orbit tribometers

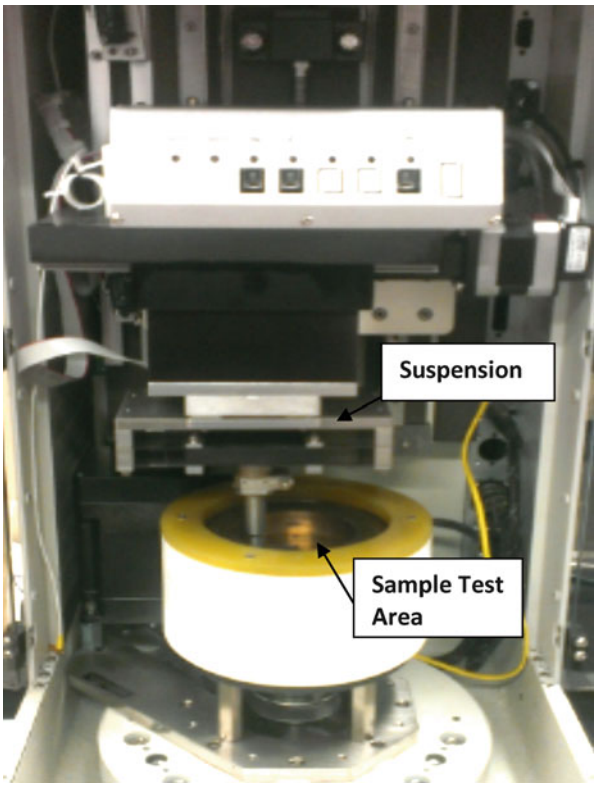

Fig. 12.16 CETR UMT multipurpose tribometer

(SOTs) used by the US National Aeronautics and Space Administration (NASA) to evaluate the performance of nano-fluid slurry lubricants under a high vacuum [125]. A schematic of the SOTs used by the NASA Glenn Research Center is shown in Fig. 12.17 [134].

3.3 Slurry Tribology Modeling

Many techniques have been developed to model the behavior of slurries in tribological applications. The challenge in modeling slurries is that particle–particle interaction and particle–fluid interaction usually play a significant role in the slurry behavior. Slurry tribology modeling has benefited from decades of fluid modeling and particle modeling from the well-developed fields such as fluid mechanics, colloid science, and granular flow.

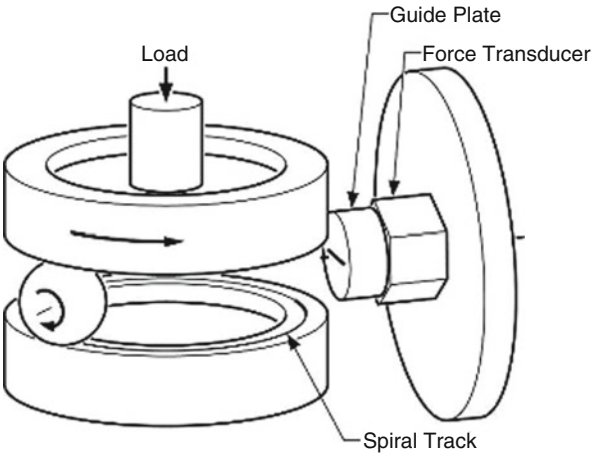

Fig. 12.17 Schematic of spiral orbit tribometer used by the NASA Glenn Research Center to test nano-fluid slurry lubrications on ball-bearing components in extreme vacuum (Courtesy NASA/GRC [134])

3.3.1 Fluid Modeling

Typically in tribology, fluids are modeled using the Reynolds equation. The Reynolds equation (12.16), derived from the more general Navier–Stokes equations, is suitable for predicting fluid pressures in thin interfaces at low Reynolds numbers [135–137]:

$$\frac{\partial}{\partial x}\left(h^3\frac{\partial p}{\partial x}\right)+\frac{\partial}{\partial y}\left(h^3\frac{\partial p}{\partial y}\right)=12\eta U\frac{dh}{dx} \tag{12.16}$$

To derive the Reynolds equation, from the Navier–Stokes equations, there are several assumptions which must be made [138]:

1. Body forces are negligible.
2. Pressure is constant through the lubricant film.
3. No slip at the bounding surfaces.
4. The lubricant flow is laminar (low Reynolds number).
5. Inertial and surface tension forces are negligible compared with viscous forces.
6. Shear stress and velocity gradients are only significant across the lubricant film.

The advent of increased computing power on modern personal computers and supercomputers has led to increased usage of computational fluid dynamics (CFD) as a means to predict fluid behavior in tribological interfaces. Because CFD is a numerical approximation of the Navier–Stokes equations (12.17 and 12.18), it is applicable for more general slurry modeling. Moreover, it is better suited for incorporating the effect of the slurry particles on the fluid:

$$\rho\left(\frac{\partial u}{\partial \mathrm{t}}+u\frac{\partial u}{\partial x}+v\frac{\partial u}{\partial y}+w\frac{\partial u}{\partial z}\right)=-\frac{\partial p}{\partial x}+\mu\left(\frac{\partial^2 u}{\partial x^2}+\frac{\partial^2 u}{\partial y^2}+\frac{\partial^2 u}{\partial z^2}\right) \tag{12.17a}$$

$$\rho\left(\frac{\partial v}{\partial \mathrm{t}}+u\frac{\partial v}{\partial x}+v\frac{\partial v}{\partial y}+w\frac{\partial v}{\partial z}\right)=-\frac{\partial p}{\partial y}+\mu\left(\frac{\partial^2 v}{\partial x^2}+\frac{\partial^2 v}{\partial y^2}+\frac{\partial^2 v}{\partial z^2}\right) \tag{12.17b}$$

$$\rho\left(\frac{\partial w}{\partial \mathrm{t}}+u\frac{\partial w}{\partial x}+v\frac{\partial w}{\partial y}+w\frac{\partial w}{\partial z}\right)=-\frac{\partial p}{\partial z}+\mu\left(\frac{\partial^2 w}{\partial x^2}+\frac{\partial^2 w}{\partial y^2}+\frac{\partial^2 w}{\partial z^2}\right) \tag{12.17c}$$

$$\frac{\partial u}{\partial x}+\frac{\partial v}{\partial y}+\frac{\partial w}{\partial z}=0 \tag{12.18}$$

In CFD, the momentum equations (12.17a–12.17c) are discretized, and pressure–velocity coupling is achieved by seeking to satisfy the continuity equation (12.18). The variables u, v, w, and p represent the x, y, z components of the fluid velocity and the pressure, respectively. The increased modeling fidelity and flexibility gained by using CFD comes at the price of computational time. As a result, when applicable, the Reynolds equation is still widely used today. As computers become faster, it is expected that CFD usage will increase in slurry tribology. Computational processing speeds may become so fast that widespread simulation of fluids in slurry tribology can be performed using molecular dynamics (MD). In MD, the fluid is not modeled as a continuum. Instead the behavior of the atoms that comprise the fluid is simulated. It is currently unfeasible to perform macroscale slurry tribology simulations using MD due to the computational resources required. However, much progress has been made in the study of nano-fluids using MD simulations at nanoscales. In the not-too-distant future, it may be possible to run an MD simulation to predict the slurry behavior at the macroscale.

3.3.2 Particle Modeling

Particle modeling in slurry tribology has benefited from a number of other fields such as contact mechanics [42] and granular flow. It is typically assumed that the behavior of the particle in the absence of the fluid will be the same as when the fluid is present except for specific forces which are introduced by the fluid. There are many numerical methods now used to predict particle behavior in slurry tribology. One of the most commonly used techniques is the discrete element method (DEM). Details about the DEM and finite element method (FEM) for particle modeling in slurry tribology are provided in the granular flow tribology section 2.3.1.

3.3.3 Particle–Fluid Interaction

The fundamentals of particle modeling in slurry tribology were developed with little consideration for the particle's effect on the fluid. Unlike classical multiphase flow mechanics where there are advanced treatments of particle dynamics, it was assumed that the particles would generally follow the path of the fluid and their

effect on the system would be to do the tribological work of removing material. This type of modeling, called one-way particle–fluid coupling, has been successful in predicting many phenomena such as material removal rates during CMP [139].

A desire to model the scenario with higher fidelity has led to the use of two-way coupling in particle tribology. In two-way coupling, the fluid is affected by forces from the particle, and the particle is affected by forces from the fluid [140]. Such interaction is necessary, especially when predicting the effect of particulates on the entrainment of lubricants into the interface between surfaces.

Typically, the momentum between the fluid and the particle is coupled by calculating the force of drag and the force of pressure gradients in the fluid (buoyancy) on the particle. In some of the earliest models, and in many models used today, Stokes drag was used to calculate the drag force. Stokes drag is applicable for spherical-particle slurry flows with low solid fractions (so that the effect of other particles can be neglected) and very low Reynolds numbers in areas where the fluid boundary has little effect on the flow around the particle. When these criteria are satisfied, Stokes drag can be calculated by 12.19:

$$F_{drag} = 6\pi\eta U a \tag{12.19}$$

When these criteria are not satisfied, it may become necessary to take into account phenomena such as the shearing of the fluid through a collection of particles and the effect of wakes generated in the fluid as it flows around the particles. For the former, there have been methods derived based on empirical predictions for the flow through packed beds of particles [141]. For the latter, more detailed modeling may be necessary, and fine CFD meshes around particles have been created to elucidate this behavior. Empirical relations, such as the COR of immersed particles [55], have also been used in slurry modeling when such relations adequately describe the dominant physics [140].

Finally, slurry tribology has benefitted largely from the field of colloid science. The understanding of forces such as Magnus forces, Saffman forces, and Brownian forces gleaned from colloid science has helped in the modeling of slurry tribology. Notably, the attractive dispersion forces (such as van der Waals forces) and the repulsive electrostatic forces (such as electric double-layer forces) are important in modeling the stability of slurries and interactions between particles.

3.4 Future Trends in Slurry Tribology

Though slurry tribology has been studied for many years, advances in the understanding of nano-fluids have opened many new applications. As discussed earlier, the introduction of nanoparticles into lubricants can help to protect bearing surfaces during boundary and mixed lubrication. Additionally, smart slurries such as magneto-rheological fluids (MR) show great promise for future implementation as their properties can be tuned based upon external magnetic fields. This property

has much potential and has already been utilized in magnetically activated suspensions. Additionally, there is a need for much analysis and modeling to be performed for these novel applications and others such as two-phase porous bearings.

4 Powder Tribology

4.1 Introduction

Powder lubricants suggest dry, cohesive, soft particles that accommodate surface velocity differences by deforming under load and adhering to surfaces. Powder lubricants can reduce friction and wear between two surfaces below boundary lubrication levels, in a manner similar to granular lubricants because of their abilities to allow interlayer motion. These similarities include the generation of lift in sliding contacts, the existence of particle density distributions, the dependence of pressure on the mixture properties, and the demonstration of slip at the boundaries in macroscale geometries [4]. However, there must be distinguishing features in the flow of powder lubricants that separate themselves from granular lubricants. One of the main differences between powder and granular lubricants is the fact that powder lubricants adhere and coat surfaces while granular lubricants slip, roll, and collide with the surfaces at their boundaries. Because granular lubricants slip, roll, and collide, granular particles experience nearly elastic collisions. On the other hand, powder particles experience entirely inelastic collisions since they adhere to surfaces after colliding with them. Another difference between powder and granular flow lies in the size of their particles (powder particles are typically on the order of 1 μm or less, while granular particles are on the order of 1 mm). This is a weaker delineation since cohesionless powders which are on the order of microns can still transfer momentum between surfaces through collisions. There are also similarities and differences between hydrodynamic fluids and powder lubricants. Similar to hydrodynamic fluids, they shear in the bulk medium, where lubrication can be attained by steady velocity accommodation. Powder lubricants can achieve this lubrication process due to their lamellar structures. However, they are different in that powder lubricants can sustain load in not only static contacts but also in flows that include parallel geometries, where the "wedge" effect is absent [4].

To understand the physics of powder lubrication, it is important to acknowledge the macroscopic and microscopic interactions of powder lubricants. Some microscopic quantities that influence powder flows are the small forces between particles, individual particle size, and porosity [142]. The interlaying bonding between the lamellar structures affects the lubrication processes of powder lubricants as supported by friction data and results gathered from an electron microscope [143]. These characteristics play a role in some important macroscopic properties,

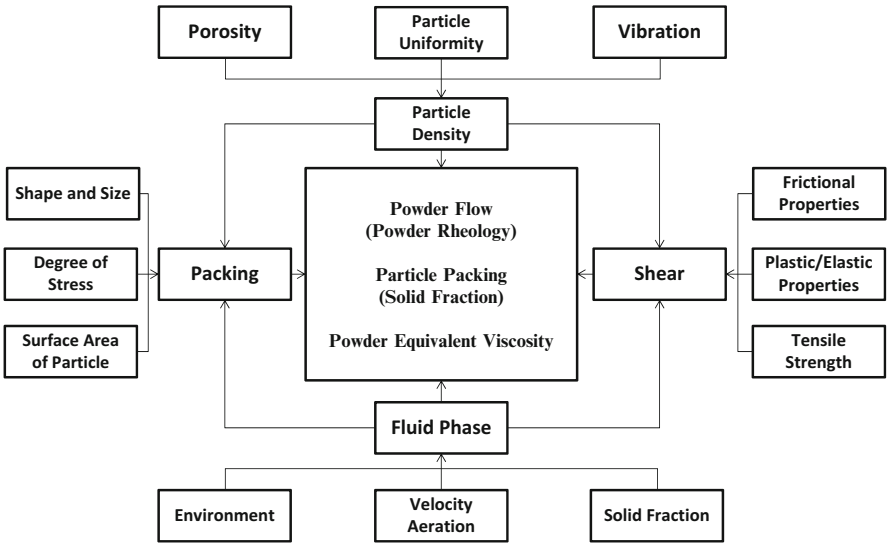

Fig. 12.18 Properties that affect powder lubricants

such as hardness and compaction. In powder lubrication, cohesive powder particles amalgamate, shear, and coat surfaces to improve lubrication performance by providing velocity accommodation and load-carrying capacity while reducing wear and friction. Figure 12.18 presents the intricacy of the dispositions that determine the circumstances of powder materials as reported by Higgs and Heshmat [144]. Some typical examples of lamellar powder lubricants include molybdenum disulfide [145, 146], titanium dioxide [147], boric acid [148], and tungsten disulfide [149].

4.2 Application and Phenomenon

Powder lubrication schemes have been proposed as innovative candidates for lubrication in extreme environments (i.e., temperature and/or loads), where conventional lubricants cannot perform adequately. For example, the increased capacity of turbine engines will result in high temperatures on the order of 800 °C, posing serious problems on modern cooling technology. At temperatures greater than 500 °C, conventional liquid lubricants are unable to sustain loads, hence, the advent of solid/particulate lubrication [4]. Kaur and Heshmat developed an oil-free journal bearing, capable of supporting significant rotor loads of 445 N (100 lb.) operating at 815 °C and 30,000 rpm that was lubricated by in situ powder film transfer. The dry particulate powders, which are pelletized, provide a long-lasting, low-power-loss backup bearing. Some applications that may use such bearings are ground- and space-based flywheel energy storage systems, auxiliary and integrated

power units, and gas turbine engines [150]. Similar concepts have been adopted by companies that manufacture several different types of self-lubricating bearings that utilize reservoirs containing polytetrafluoroethylene (PTFE) solid lubricants for aerospace, hydropower, industrial, and offshore applications.

Powder lubricant applications extend beyond the bearing domain. Heshmat designed a powder lubricant piston ring for adiabatic diesel engines and coal–water slurry-fueled diesel engines [151]. The heat transfer between the cylinder walls and the cooling system must be minimized in order to achieve an adiabatic cycle in an internal combustion engine such as a diesel engine. The heat transfer normally makes up for 30–35 % of the total fuel energy of a diesel cycle. An increase in surface temperatures at the piston is observed in this configuration during the compression stage. As the surface temperatures exceed the limit of the operational temperature for the engine oil, current adiabatic diesel cycles are reduced to keep the temperature of the process below the limit of the operational temperature of the hydrocarbon lubricant. The reduction of the engine's capacity results in lower fuel efficiency and lower power per unit weight.

Consequently, a powder-lubricated piston ring was proposed for an adiabatic cycle diesel engine that can operate at temperatures above the hydrocarbon lubrication limit of 600 °C, thus, permitting the engine to function with higher fuel efficiency and higher power output [151]. There are two embodiments of the patent. The first includes powder-lubricated piston rings in conjunction with hydrodynamic compliant-mounted bearings, and the second includes powder-lubricated piston rings in conjunction with oil-lubricated hydrodynamic rings. Quasi-hydrodynamic lubricant film between the piston and the cylinder is formed to provide a separation between the two surfaces. The flow of powder particles is similar to the motion of liquid molecules, such as hydrocarbon lubricant; the powder particulates provide a load-carrying capacity and film thickness.

Powder lubrication can also be seen as an important factor in the fault weakening of earthquake phenomenon [152]. For a long time, earthquake instability has been accredited to fault weakening during accelerated slip, and the main question of earthquake physics has revolved around identifying the weakening mechanisms. During experiments with dry solid-granite blocks, fine rock powder, known as gouge, quickly forms and is responsible for the reduced fault strength due to its organization into a thin deforming layer. When the gouge ages, which happens soon after slip, the fault would regain its strength rapidly, thereby, suggesting that only newly formed gouge can weaken the experimental faults. It can be observed that dynamic gouge formation is a common and causal mechanism for an earthquake due to the behavior similarity between a fault gouge and industrial powder lubricants.

4.3 Experiments

The evaluation of powder lubrication based on its frictional behavior and wear characteristics has been studied extensively. Various powder lubrication parameters such as materials, surface conditions, load, speed, temperature, environment,

contact area, and particle size are the main subjects of studies [153–155]. This section will explore some of the experimental approaches to determine the relationship between some of the mentioned parameters in both thick film (i.e., hydrodynamic lubrication) and thin film (i.e., boundary lubrication) types of powder lubrication.

4.3.1 Thick Film Powder Lubrication

One of the earliest thick film experimental investigations was carried out by Heshmat to present a visual documentation of the fluid-like flow of certain powders [119]. It can be observed that a number of basic features of powder flow in narrow interfaces exhibit the characteristics of fluid film lubrication. These characteristics are also called the "quasi-hydrodynamic" nature of powder lubricants. The test rig assembly designed for flow visualization included a variable speed electric motor and a cup-shaped transparent journal bearing. The test rig and journal were made of a transparent thermoplastic synthetic resin (methyl methacrylate). A steel shaft was connected at the journal's center. An outboard grease-lubricated bushing radially provided the support for the rotating shaft. A transparent cup-shaped cover was positioned over the journal bearing to minimize the powder loss during the test [119]. Figure 12.19 shows the general experimental setup.

The test rig was utilized to conduct a series of experiments to explore several features of powder flow in eccentrically convergent spaces. The transparent bearing clearance was filled with titanium dioxide (TiO_2) and molybdenum disulfide (MoS_2) powders in a layered manner. To provide a reference frame for the powder testing, the basic pattern of fluid flow in the interface of a journal bearing was demonstrated. Viscosity was the main fluid property that was responsible for the behavior of a hydrodynamic film; thereby, paint, due to its high viscosity that is equivalent to SAE 40 oil, was chosen to compare to the hydrodynamic flow of the powder lubricant. In comparing the results between powder flow and fluid flow in a journal bearing, the following was inferred for powder flow [119]:

- A boundary layer-like flow can be observed along the moving surface, and there is a distribution of shear stress across the film.
- Due to the journal rotation, compressive and tensile stresses in the radial direction are generated in the film. The converging region of the film forms compressive stresses, and the diverging region produces tensile stresses.
- There was an evidence of the formation of hydrodynamic pressure profiles in powder lubricants.
- The original circumferential flow of powder assumes an axial motion as the powder moves towards the smallest gap in the converging section. This occurrence suggests an axial pressure distribution, which is analogous to hydrodynamic lubrication.
- After the powder particulates flow passed the smallest gap of the converging section, a powder film shows chaotic motion similar to turbulent flow.

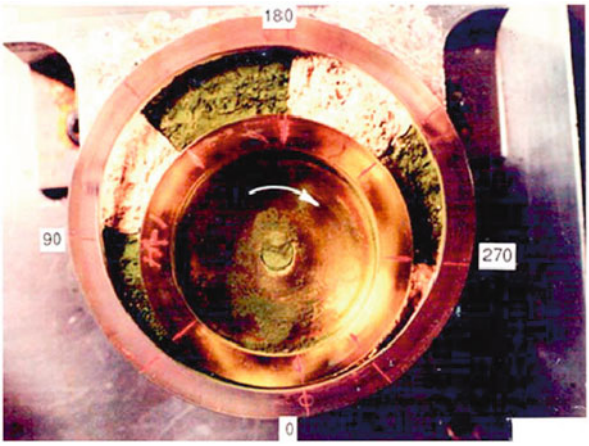

Fig. 12.19 Thick film powder-lubricated journal bearing

- There was adhesion of a thin powder layer to the two mating surfaces that was responsible for the low-friction behavior of the tribological process of powder lubrication.

A follow-on series of work to the powder-lubricated bearing visualization studies led Heshmat to develop what he called "quasi-hydrodynamic theory of powders" in converging contacts [156].

4.3.2 Thin Film Powder Lubrication

Heshmat and his collaborators studied powders in pin-on-disk tests to evaluate the performance of molybdenum disulfide (MoS_2) in bearings [150, 157]. The "pellet-on-disk" tests were performed using a modified pin-on-disk tribometer where compacted MoS_2 powder was run against a titanium carbide (TiC) disk. The two major technology components for the experimental setup consisted of the pelletized powder lubricant delivery system and the compliantly mounted slider type. The tests helped to establish the optimum geometries and system parameters to make MoS_2 lubricant pellets [147]. From this work, a self-contained solid-/powder-lubricated auxiliary hydrodynamic bearing was developed. This bearing was operated at 30,000 rpm and at loads up to 445 N (100 lb) [150].

Similar to the pellet-on-disk with slider tribometer developed by Heshmat, Higgs and Wornyoh developed a tribometer setup to study thin powder transfer films from compacted powder pellets [158], as shown in Fig. 12.20. In wear tests, MoS_2 pellets were sheared against the surface of the rotating titanium carbide (TiC) disk forming a transfer film which was then depleted by the downstream loaded slider pad [158]. The resulting friction coefficient between the slider and disk was a function of the amount of lubricant that remained on the disk.

During the tests, a pellet was loaded against the disk, as it rotated. Since the pellet is pressed against the disk with a weight F_p, the thin film is transferred to the

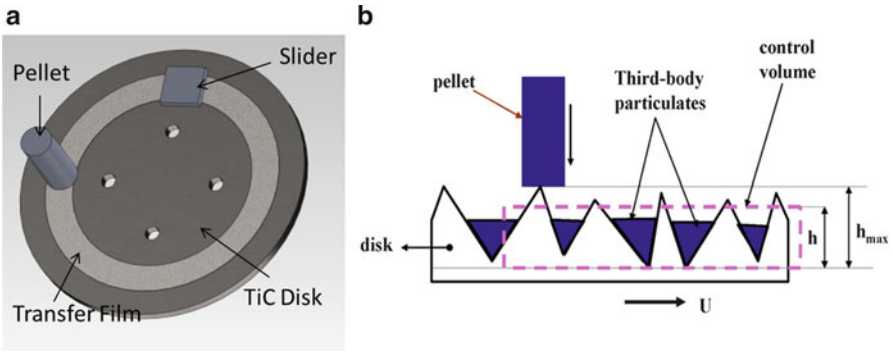

Fig. 12.20 (**a**) Pellet-on-disk with slider setup. (**b**) Diagram of the pellet–disk and slider/disk interfaces

disk which has a linear speed U. The transfer film supports the normal load F_s on the slider. Lastly, the wear rate of the pellet and the frictional behavior at the pellet–disk and pad/disk interfaces were measured with load cells [158].

Figure 12.21 shows typical experimental results from the pellet-on-disk with slider tribometer. In Fig. 12.21a, the friction coefficients for an MoS_2 pellet with an average particle size of 7.4 μm and slider riding atop the rotating disk are shown. The friction coefficient for the solid MoS_2 compact is generally higher than a hard metal slider pad riding on a lubricious transfer film of MoS_2 likely because the slider pad shears the lamellar MoS_2 film similar to a fluid. Figure 12.21b shows a typical wear graph for the pellet in terms of mass loss in grams. In Fig. 12.21c, the friction coefficients for an MoS_2 pellet with an average particle size of 1.56 μm and slider are shown. The friction coefficients reach steady-state values in approximate range of 0.13 and 0.15. The distance that it takes for these friction coefficients to reach the steady-state values corresponds to the distance that indicates where a steady-state wear rate starts to occur, and the approximate distance falls at 1 km as shown in Fig. 12.21d.

4.4 Modeling

The nonexistence of a clear-cut fundamental equation of motion for powder lubrication led researchers to adopt a variety of forms [4]. For example, some authors have favored the rheological study or the study of material as a reasonable assumption in modeling powder lubrication [4]. Rheology combines the theories of continuum mechanics with ideas obtained by considering the microstructure of the objects being studied. This section will examine three different modeling approaches such as thick film modeling, thin film modeling, and discrete element method (DEM) modeling.

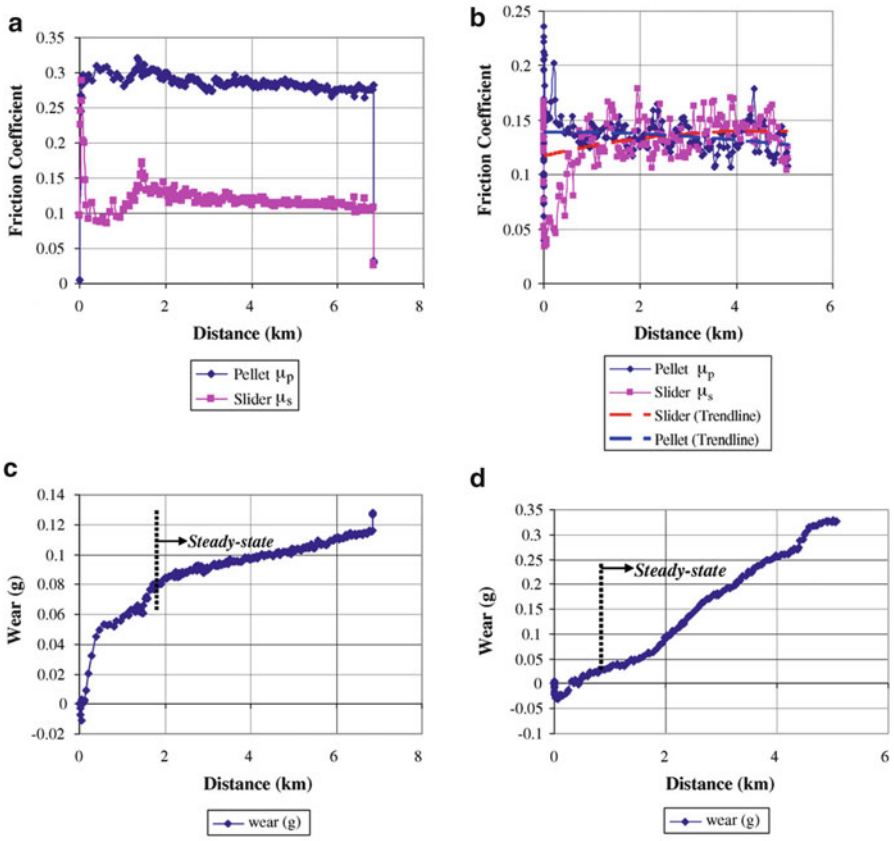

Fig. 12.21 Test results from pellet-on-disk test. (**a**, **c**) Pellet and slider pad friction coefficient. (**b**, **d**) Cumulative pellet wear. (**a**, **b**) Test results for average MoS_2 powder particle size of 7.4 μm. (**c**, **d**) Test results for average MoS_2 powder particle size of 1.56 μm

4.4.1 Thick Film Powder Lubrication Modeling

For thick film powder films, Heshmat [159] used a continuum approach to develop a semiempirical model to predict the behavior and performance of powders, which he said behaved as "quasi-hydrodynamic" lubricant films. Figure 12.22 shows his phenomenological description of the velocity accommodation provided by lamellar powders between sliding surfaces. Lamellar powders such as MoS_2, graphite, and tungsten disulfide are called "powder lubricants" because they inherently have layered shearing. Heshmat developed a rheological model for powder lubricants which related the shear rate (du/dy) of the powder to an odd fifth-order function of the shear stress τ as seen in (12.20) [159]. Powder lubrication or layered shearing was shown to only occur when the film is sheared with a stress between the powder's shear-based yield strength τ_0 and its limiting shear stress τ_l; both are values which he measured experimentally [159]:

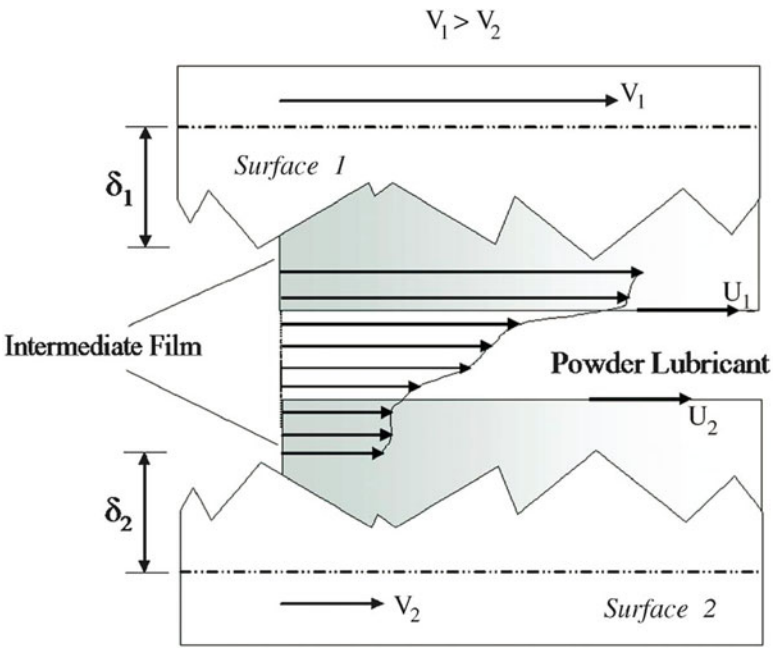

Fig. 12.22 Powder lubricant as a third body

$$\mu\left(\frac{du}{dy}\right) - \tau_0 = \tau + C_1\tau^3 + C_2\tau^5 \tag{12.20}$$

where μ is the powder viscosity, u is the velocity, τ_o is the yield shear strength, τ is the shear stress, and C_1 and C_2 are empirical constants. An effective powder viscosity could be measured in rheological-type experiments, and a one-dimensional momentum equation taken from the Navier–Stokes fluid equations was used to determine the hydrodynamic pressure numerically.

4.4.2 Thin (Transfer) Film Powder Lubrication Modeling

The transfer film approach of modeling powder lubrication assumes the powder film thickness does not exceed the height of the surface asperities and, in most cases, is less than the tallest asperities (see Fig. 12.20b). In order to develop a tribology model of the lubrication process, the asperity domain was assumed to be the control volume [158]. Figure 12.20b showed a simplified schematic of the pellet as it is sheared against the disk and as the slider pad depletes the lubricant off the disk with exaggerated asperity heights; for simplicity, the slider is not shown. A control volume fractional coverage (CVFC) model [158] was developed with the following assumptions:

- The slider/disk and pellet–disk interface topographies are represented by a nominally flat or slider surface in contact with a rough disk.
- The disk topography varies little relative to the maximum asperity height h_{max}.
- The frictional response in the pellet–disk and slider/disk interfaces is predominantly a function of the height of the transfer film covering the disk surface.

The fractional coverage, X, is dimensionless and is defined as the fraction of lubricant that covers the asperities of the disk surface. That is,

$$X = h/h_{\max} \tag{12.21}$$

where h is the local height of third body film. The film height when the disk asperities are completely covered is $h = h_{max}$ and in that case, $X = 1$. Similarly, $X = 0$ represents the case of no lubricant coverage. Referring to Fig. 12.20b, consider the control volume that encloses asperities and valleys. The rate at which the amount of lubricant can be stored on the disk is equal to the difference between the amount of lubricant entering the control volume and the amount of lubricant exiting the control volume. This is expressed as (12.22) as a conservation of mass flow rate or volume flow rate if density is assumed constant as in this case:

$$\begin{aligned}(\textit{Third Body Storage Rate}) = (\textit{Third Body Input Rate}) \\ - (\textit{Third Body Output Rate})\end{aligned} \tag{12.22}$$

To mathematically interpret (12.21), a generalized wear law is used to describe the rates of material being input or output from the control due to wear mechanisms:

$$\dot{V} = KF_N U \tag{12.23}$$

where $\dot{V}$ is the volume wear rate, K is the dimensional wear coefficient, F_N is the normal load applied, and U is the sliding velocity. K is an empirical constant that describes the probability of wear occurring between two different materials such as TiC on MoS_2, although in some cases, K could just be between the same kinds of material (e.g., MoS_2 pellet riding on MoS_2 third body). Applying Archard's wear law from (12.23) on each of the interacting interfaces, (12.22) becomes

$$A\frac{dh}{dt} = K_p F_p U(1 - X) - K_{ep} F_p U(X) - K_{es} F_s U(X) \tag{12.24}$$

where A is the cross-sectional area and F_p and F_s are pellet and slider loads, respectively. Additionally, K_p is the wear coefficient for the pellet–disk interface, while wear coefficients for the third body wear due to the shearing from the pellet and slider pad are K_{ep} and K_{es}. The fractional coverage X coefficients in each of the three terms on the right side of (12.24) act as "switches." For example, if the disk is fully covered ($X = 1$), the pellet switches off from wearing which means the first term goes to zero. When the disk has no lubricant film on it (X = 0), the second and

third output wear terms on the right side of the equation go to zero, and the equation reduces back to the general wear equation just for the pellet.

Equation (12.24) is the governing equation which together with the initial condition $X(0) = 0$ completely define the problem for the CVFC model. The solution to (12.24) is given by

$$X(t) = \frac{(K_p F_p)}{(K_{ep} + K_p)F_p + K_{es}F_s}\left[1 - \exp\left(-\frac{t}{\tau}\right)\right] \tag{12.25}$$

where τ is the time constant defined by

$$\tau = \frac{Ah_{\max}}{\left((K_{ep} + K_p)F_p + K_{es}F_s\right)U} \tag{12.26}$$

After a long time has elapsed, the steady-state fractional coverage is

$$X_{ss} = \frac{(K_p F_p)}{(K_{ep} + K_p)F_p + K_{es}F_s} \tag{12.27}$$

Assuming a linear rule of mixture can be used to predict the friction coefficient between unlubricated and fully lubricated conditions, the pellet and slider friction coefficients can be defined as (12.28) and (12.29):

$$\mu_p = X\mu_{lub,p} + (1 - X)\mu_{dry,p} \tag{12.28}$$

$$\mu_s = X\mu_{lub,s} + (1 - X)\mu_{dry,s} \tag{12.29}$$

where μ_p and μ_s are friction coefficients at the pellet–disk and slider/disk interfaces, respectively. The pellet and slider friction coefficients for unlubricated conditions are $\mu_{dry,p}$ and $\mu_{dry,s}$, while those for lubricated conditions are indicated by $\mu_{lub,p}$ and $\mu_{lub,s}$.

Lastly, Iordanoff et al. [160] suggest the use of a discrete element method (DEM) modeling approach. They studied mechanisms operating in sliding contacts and outline the influence of external parameters. The proposed unified approach considers the following conventional modeling:

- The quasi-hydrodynamic model developed by Heshmat [159]
- The kinetic model developed by Haff [109] and extensively modified by tribologists, such as Dai et al. [161], McKeague and Khonsari [5, 162], Yu, et al. [163], and Zhou and Khonsari [108]

The authors' [160] discrete model was based on the principles of DEM proposed by Cundall and Strack [72] for geotechnical applications. Recently, simulations involving solid third bodies, similar to pelletized powder, have been conducted by Fillot et al. [164].

5 Conclusion

The purpose of this chapter was to expose readers to the tribology of particles interacting with other particles, fluids, and external or internal surfaces. The topic of particle tribology is much broader than the three tribosystems—granular, slurry, and powder—presented in this chapter. However, most fundamental issues concerning particle tribology and its associated applications likely have been addressed within the sections of this chapter. For example, granular flows can be a broad description of particulate systems where the particles primarily interact through collisions resulting in dissipative momentum transfer. An application of this might be the flow of coal down long pipelines where vast amounts of power are needed to pump these solids which are constantly losing kinetic energy due to particle–particle and particle–surface interactions. Slurry flows which are multiphase particle–fluid flows exhibit behavior that is often difficult to predict because one must first understand the fluid mechanics and particle dynamics occurring between sliding surfaces. And finally, the most classical of the particle tribology areas is powder lubrication which refers to particles that often exhibit dual lubrication behavior. They either accommodate surface velocity differences by shearing, or they lower frictional performance by coating surface asperities during sliding. The student aiming to study broad particle engineering and science problems such as earthquake prediction, flow stoppage during solids processing, and the erosion susceptibility of surfaces during processing or basic operation should greatly benefit from the concepts presented in this chapter.

References

1. Higgs CF, Tichy J (2004) Granular flow lubrication: continuum modeling of shear behavior. J Tribol 126(3):499–510
2. Yu C-M, Craig K, Tichy J (1994) Granular collision lubrication. J Rheol 38(4):921–936
3. Elkholy KN, Khonsari MM (2007) Granular collision lubrication: experimental investigation and comparison to theory. J Tribol 129(4):923
4. Wornyoh EYA, Jasti VK, Fred Higgs C (2007) A review of dry particulate lubrication: powder and granular materials. J Tribol 129(2):438
5. McKeague KT, Khonsari MM (1996) An analysis of powder lubricated slider bearings. J Tribol 188(1):206–214
6. Iordanoff I, Khonsari MM (2004) Granular lubrication: toward an understanding of the transition between kinetic and quasi-fluid regime. J Tribol 126(1):137
7. Lu K, Brodsky EE, Kavehpour HP. Tribological aspects and fluidity of dense granular flow. In: 2005 ASME international mechanical engineering congress and exposition 2005. American Society of Mechanical Engineers: Orlando, FL, United States. pp 181–190
8. Roberts AW, Ooms M, Wiche SJ (1990) Concepts of boundary friction adhesion and wear in bulk solids handling. Bulk Solids Handling 10(2):189–198
9. Lee T, Jia L (2003) Particle attrition by particle-surface friction in dryers. Pharm Technol 27(5):64–72

10. Higgs III CF, Jasti V, Racusen C, Heller C, Cohen N, Tichy J (2006) On the behavior of granular materials in rough wheel contacts on mars. In: Tenth biennial ASCE aerospace division international conference on engineering, construction, and operations in challenging environments 2006, American Society of Civil Engineers. p. 32
11. Elliott KE, Ahmadi G, Kvasnak W (1998) Couette flows of a granular monolayer—an experimental study. J Non-Newtonian Fluid Mech 74(1):89–111
12. May LBH, Golick LA, Phillips KC, Shearer M, Daniels KE (2010) Shear-driven size segregation of granular materials: modeling and experiment. Phys Rev E 81(5):051301
13. Golick L, Daniels K (2009) Mixing and segregation rates in sheared granular materials. Phys Rev E 80(4):042301
14. Wambaugh J, Behringer R, Matthews J, Gremaud P (2007) Response to perturbations for granular flow in a hopper. Phys Rev E 76(5):051303-1–051303-8
15. To K, Lai P-Y, Pak H (2001) Jamming of granular flow in a two-dimensional hopper. Phys Rev Lett 86(1):71–74
16. Samadani A, Pradhan A, Kudrolli A (1999) Size segregation of granular matter in silo discharges. Phys Rev E 60(6):7203–7209
17. Dhoriyani M, Jonnalagadda K, Kandikatla R, Rao K (2006) Silo music: sound emission during the flow of granular materials through tubes. Powder Technol 167(2):55–71
18. Ottino JM, Khakhar DV (2000) Mixing and segregation of granular materials. Annu Rev Fluid Mech 32:55–91
19. Gray JMNT, Ancey C (2009) Segregation, recirculation and deposition of coarse particles near two-dimensional avalanche fronts. J Fluid Mech 629:387
20. Arteaga P, Tuzun U (1990) Flow of binary mixtures of equal-density granules in hoppers—size segregation, flowing density and discharge rates. Chem Eng Sci 45(1):205–223
21. Ketterhagen W, Curtis J, Wassgren C, Kong A, Narayan P, Hancock B (2007) Granular segregation in discharging cylindrical hoppers: a discrete element and experimental study. Chem Eng Sci 62(22):6423–6439
22. Samadani A, Kudrolli A (2001) Angle of repose and segregation in cohesive granular matter. Phys Rev E 64(5):051301
23. Conway SL, Lekhal A, Khinast JG, Glasser BJ (2005) Granular flow and segregation in a four-bladed mixer. Chem Eng Sci 60(24):7091–7107
24. May LBH, Shearer M, Daniels KE (2010) Scalar conservation laws with nonconstant coefficients with application to particle size segregation in granular flow. J Nonlinear Sci 20(6):689–707
25. Hong DC, McLennan JA (1992) Molecular dynamics simulations of hard sphere granular particles. Physica A 187(1):159–171
26. Corwin EI, Jaeger HM, Nagel SR (2005) Structural signature of jamming in granular media. Nature 435(7045):1075–1078
27. Garcimartín A, Zuriguel I, Maza D, Pastor JM, Pugnaloni LA. Jamming in granular matter. In: 8th Experimental Chaos Conference2004, AIP Conference Proceedings, American Institute of Physics, Florence, Italy. pp 279–288
28. Zhang J, Majmudar TS, Sperl M, Behringer RP (2010) Jamming for a 2D granular material. Soft Matter 6(13):2982
29. Mailman M, Schreck C, O'Hern C, Chakraborty B (2009) Jamming in systems composed of frictionless ellipse-shaped particles. Phys Rev Lett 102(25):255501
30. Schreck CF, Xu N, O'Hern CS (2010) A comparison of jamming behavior in systems composed of dimer- and ellipse-shaped particles. Soft Matter 6(13):2960
31. Liu AJ, Nagel SR (1998) Jamming is not just cool any more. Nature 396:21–22
32. Shibly H, Iagnemma K, Dubowsky S (2005) An equivalent soil mechanics formulation for rigid wheels in deformable terrain, with application to planetary exploration rovers. J Terramech 42(1):1–13
33. Liu J, Tang S, Cheng P, Liu S (2012) Influence analysis and evaluation of wheel parameters on motion performance of lunar rover. Inform Technol J 11(2):225–232

34. Ding L, Deng Z, Gao H, Nagatani K, Yoshida K (2010) Planetary rovers' wheel–soil interaction mechanics: new challenges and applications for wheeled mobile robots. Intell Serv Robot 4(1):17–38
35. Marinack MC Jr, Jasti VK, Choi YE, Higgs CF (2011) Couette grain flow experiments: the effects of the coefficient of restitution, global solid fraction, and materials. Powder Technol 211(1):144–155
36. Sondergaard R, Chaney K, Brennen CE (1990) Measurements of solid spheres bouncing off flat plates. J Appl Mech Trans ASME 57(3):694–699
37. Kharaz AH, Gorham DA (2000) A study of the restitution coefficient in elastic-plastic impact. Philos Mag Lett 80(8):549–559
38. Koller MG, Kolsky H (1987) Waves produced by the elastic impact of spheres on thick plates. Int J Solid Struct 23(10):1387–1400
39. Reed J (1985) Energy losses due to elastic wave propagation during an elastic impact. J Phys D Appl Phys 18(12):2329–2337
40. Tabor D (1948) A simple theory of static and dynamic hardness. Proc R Soc A192:247
41. Vincent JH (1900) Experiments on impact. Proc Camb Philos Soc 10:332–357
42. Johnson KL (1985) Contact mechanics. Cambridge University Press, Cambridge, UK
43. Tabor D (1951) The hardness of metals. Oxford University Press, London
44. Seifried R, Schiehlen W, Eberhard P (2005) Numerical and experimental evaluation of the coefficient of restitution for repeated impacts. Int J Impact Eng 32(1):508–524
45. Raman CV (1920) On some applications of Hertz's theory of impact. Phys Rev 15:249–343
46. Marinack Jr MC, Gaudio BG, Musgrave RE, Rizzo CE, Lovell M, Higgs III CF (2010) Coefficient of restitution testing: explicit finite element modeling and experiments. In: ASME/STLE 2010 International Joint Tribology Conference 2010, Conference Proceedings, San Francisco, CA
47. Marinack Jr MC, Musgrave RE, Higgs III CF (2012) Experimental investigations on the coefficient of restitution of single particles. Tribol Trans. Accepted for publication
48. Minamoto H, Hagawa T, Kawamura S (2010) Direct central impact between two spheres made of dissimilar materials. Nihon Kikai Gakkai Ronbunshu, C Hen (Trans Jpn Soc Mech Eng C) 76(768):1988–1995
49. Minamoto H, Kawamura S (2011) Moderately high speed impact of two identical spheres. Int J Impact Eng 38(2):123–129
50. Goldsmith W (1960) Impact. E. Arnold Pub, London, pp 249–307
51. Dong H, Moys M (2006) Experimental study of oblique impacts with initial spin. Powder Technol 161(1):22–31
52. Foerster SF, Louge MY, Chang H, Allia K (1994) Measurements of the Collision Properties of Small Spheres. Phys Fluids 6(3):1108–1115
53. Kharaz AH, Gorham DA, Salman AD (2001) An experimental study of the elastic rebound of spheres. Powder Technol 120(3):281–291
54. Gondret P, Lance M, Petit L (2002) Bouncing motion of spherical particles in fluids. Phys Fluids 14(2):643
55. Joseph GG, Zenit R, Hunt ML, Rosenwinkel AM (2001) Particle-wall collisions in a viscous fluid. J Fluid Mech 433:329–346
56. Ruiz-Angulo A, Hunt ML (2010) Measurements of the coefficient of restitution for particle collisions with ductile surfaces in a liquid. Granular Matter 12(2):185–191
57. Bagnold RA (1954) Experiments on a gravity-free dispersion of large spheres in a newtonian fluid under shear. Proc R Soc Lond A Math Phys Sci 225(1160):49–63
58. da Cruz F (2004) Friction and jamming in granular flows. Ecole Nationale des Ponts et Chaussees, Marne la vallee
59. Mueth DM, Debregeas GF, Karczmar GS, Eng PJ, Nagel SR, Jaeger HM (2000) Signatures of granular microstructure in dense shear flows. Nature 406(6794):385–389
60. Bocquet L, Losert W, Schalk D, Lubensky T, Gollub J (2001) Granular shear flow dynamics and forces: experiment and continuum theory. Phys Rev E 65(1):011307

61. MiDi G (2004) On dense granular flows. Eur Phys J E 14(4):341–365
62. Tardos GI, Khan MI, Schaeffer DG (1998) Forces on a slowly rotating, rough cylinder in a couette device containing a dry frictional powder. Phys Fluids 10(2):335–341
63. Veje CT, Howell DW, Behringer RP (1999) Kinematics of a two-dimensional granular Couette experiment at the transition to shearing. Phys Rev E 59(1):739–745
64. Howell DW, Behringer RP, Veje CT (1999) Fluctuations in granular media. Chaos 9 (3):559–572
65. Losert W, Bocquet L, Lubensky TC, Gollub JP (2000) Particle dynamics in sheared granular matter. Phys Rev Lett 85(7):1428–1431
66. Jasti V, Higgs C (2008) Experimental study of granular flows in a rough annular shear cell. Phys Rev E 78(4):041306
67. Savage SB, Sayed M (1984) Stresses developed by dry cohesionless granular materials sheared in an annular shear cell. J Fluid Mech 142:391–430
68. Hanes DM, Inman DL (1985) Observations of rapidly flowing granular-fluid materials. J Fluid Mech 150:357–380
69. Miller B, O'Hern C, Behringer RP (1996) Stress fluctuations for continuously sheared granular materials. Phys Rev Lett 77(15):3110–3113
70. Craig K, Buckholz RH, Domoto G (1986) Experimental study of the rapid flow of dry cohesionless metal powders. J Appl Mech Trans ASME 53(4):935–942
71. Craig K, Buckholz RH, Domoto G (1987) Effect of shear surface boundaries on stress for shearing flow of dry metal powders—an experimental study. J Tribol 109(2):232–237
72. Cundall PA, Strack ODL (1979) Discrete numerical model for granular assemblies. Geotechnique 29(1):47–65
73. Walton OR (1994) Numerical simulation of inelastic. Frictional particle-particle interactions. In: Roco MC (ed) Particulate two-phase flow. Butterworth-Heinemann, Stoneham, pp 884–911
74. Hawkins GW (1983) Simulation of granular flow. In: Jenkins JT, Satake M (eds) Mechanics of granular materials: new models and constitutive relations. Elsevier Science Publications, Amsterdam, pp 305–312
75. Hopkins MA, Shen HH (1988) A Monte Carlo simulation of a simple shear flow of granular materials. In: Satake M, Jenkins JT (eds) Micromechanics of granular materials. Elsevier Science Publications, Amsterdam
76. Campbell CS, Brennen CE (1985) Computer simulation of granular shear flows. J Fluid Mech 151:167–188
77. Hopkins MA, Louge MY (1991) Inelastic microstructure in rapid granular flows of smooth disks. Phys Fluids A 3(1):47–57
78. Jenkins JT, Richman MW (1988) Plane simple shear of smooth inelastic circular disks: the anisotropy of the second moment in the dilute and dense limits. J Fluid Mech 192:313–328
79. Sawyer WG, Tichy JA (2001) Lubrication with granular flow: continuum theory, particle simulations. Comp Exp J Tribol 123(4):777
80. Yu C-M, Tichy J (1996) Granular collision lubrication: effect of surface roughness, particle size and solids fraction. Tribol Trans 39(3):537–546
81. Louge MY (1994) Computer simulations of rapid granular flows of spheres interacting with a flat, frictional boundary. Phys Fluids 6(7):2253
82. Jenkins JT (1992) Boundary conditions for rapid granular flow: flat frictional walls. J Appl Mech 59(1):120–127
83. McCarthy JJ, Jasti V, Marinack M, Higgs CF (2010) Quantitative validation of the discrete element method using an annular shear cell. Powder Technol 203(1):70–77
84. Von Neumann J (1966) Theory of self-reproducing automata. In: Burks AW (ed.) University of Illinois Press, Urbana
85. Ilachinski A (2001) Cellular automata a discrete universe. World Scientific Publishing Co. Pte. Ltd., Singapore

86. Marinack MC Jr, Mpagazehe JN, Higgs CF III (2012) An Eulerian, lattice-based cellular automata approach for modeling multiphase flows. Powder Technol 221:47–56
87. Jasti VK, Higgs CF (2010) A fast first order model of a rough annular shear cell using cellular automata. Granular Matter 12(1):97–106
88. Fitt AD, Wilmott P (1992) Cellular-automaton model for segregation of a two-species granular flow. Phys Rev A 45(4):2383
89. Karolyi A, Kertesz J, Havlin S, Makse HA, Stanley HE (1998) Filling a silo with a mixture of grains: friction-induced segregation. Europhys Lett 44(3):386–392
90. Cizeau P, Makse HA, Stanley HE (1999) Mechanisms of granular spontaneous stratification and segregation in two-dimensional silos. Phys Rev E 59(4):4408–4421
91. Alonso JJ, Herrmann HJ (1996) Shape of the tail of a two-dimensional sandpile. Phys Rev Lett 76(26):4911–4914
92. Goles E (1992) Sand pile automata. Ann l'Instit Henri Poincare Phys Theor 56(1):75–90
93. Karolyi A, Kertesz J (1998) Lattice-gas model of avalanches in a granular pile. Phys Rev E 57(1):852–856
94. Kozicki J, Tejchman J (2005) Application of a cellular automaton to simulations of granular flow in silos. Granular Matter 7(1):45–54
95. Baxter WG, Behringer RP (1990) Cellular automata models of granular flow. Phys Rev A 42(2):1017–1020
96. Marinack MC Jr, Higgs CF III (2011) The inclusion of friction in lattice-based cellular automata modeling of granular flows. J Tribol 133(3):031302
97. Jasti VK, Higgs CF (2006) A lattice-based cellular automata modeling approach for granular flow lubrication. J Tribol 128(2):358
98. Österle W, Dmitriev AI, Kloß H (2012) Possible impacts of third body nanostructures on friction performance during dry sliding determined by computer simulation based on the method of movable cellular automata. Tribol Int 12(48):128–136
99. Tavarez FA (2001) Simulation behavior of composite grid reinforced concrete beams using explicit finite element methods. University of Wisconsin-Madison, Madison, WI
100. Kabir MA, Lovell MR, Higgs CF (2008) Utilizing the explicit finite element method for studying granular flows. Tribol Lett 29(2):85–94
101. Kabir MA, Jasti VK, Higgs CF, Lovell MR (2008) An evaluation of the explicit finite-element method approach for modelling dense flows of discrete grains in a Couette shear cell. Proc Inst Mech Eng J J Eng Tribol 222(6):715–723
102. Wu C-Y, Li L-Y, Thornton C (2005) Energy dissipation during normal impact of elastic and elastic-plastic spheres. Int J Impact Eng 32(1):593–604
103. Seifried R, Minamoto H, Eberhard P (2010) Viscoplastic effects occurring in impacts of aluminum and steel bodies and their influence on the coefficient of restitution. J Appl Mech 77(4):041008
104. Li L-y, Thornton C, Wu C-y (2000) Impact behaviour of elastoplastic spheres with a rigid wall. Proc Inst Mech Eng C J Mech Eng Sci 214(8):1107–1114
105. Katta RR, Polycarpou AA, Hanchi JV, Crone RM (2009) High velocity oblique impact and coefficient of restitution for head disk interface operational shock. J Tribol 131(2):021903
106. ANSYS (2005) Ansys, LS-DYNA user's guide (release 10). Ansys, Inc., Livermore, CA
107. Tsai H-J, Jeng Y-R (2006) Characteristics of powder lubricated finite-width journal bearings: a hydrodynamic analysis. J Tribol 128(2):351
108. Zhou L, Khonsari MM (2000) Flow characteristics of a powder lubricant sheared between parallel plates. J Tribol 122(1):147–154
109. Haff PK (1983) Grain flow as a fluid-mechanical phenomenon. J Fluid Mech 134:401–430
110. Lun CKK, Savage SB, Jeffrey DJ, Chepurniy N (1984) Kinetic theories for granular flow: inelastic particles in couette flow and slightly inelastic particles in a general flowfield. J Fluid Mech 140:223–256
111. Higgs CF III (2001) Particulate flow lubrication: continuum modeling of shear behavior. Department of Mechanical Engineering, Rensselaer Polytechnic Institute, Troy, NY

112. Elrod HG (1988) Granular flow as a tribological mechanism—a first look. In: Interface Dynamics, Proc. of the Leeds-Lyon Conference, Butterworth, Oxford, England. p. 75
113. Dai F, Khonsari MM, Lu ZY (1994) On the lubrication mechanism of grain flows. STLE Tribol Trans 37(3):516–524
114. Heshmat H (1992) The quasi-hydrodynamic mechanism of powder lubrication. Part II: lubricant film pressure profile. Lubr Eng 48(5):373–383
115. Pappur M, Khonsari MM (2003) Flow characterization and performance of a powder lubricated slider bearing. J Tribol 125(1):135
116. Jenkins JT, Richman MW (1985) Kinetic theory for plane flows of a dense gas of identical, rough, inelastic, circular disks. Phys Fluids 28(12):3485
117. Hui K, Haff PK, Ungar JE, Jackson R (1984) Boundary conditions for high-shear grain flows. J Fluid Mech 145:223–233
118. Wyszynski ML, Bridgewater J (1993) Effect of solid lubricants on powder attrition and breakage. Tribol Int 26(5):311–317
119. Heshmat H (1992) The quasi-hydrodynamic mechanism of powder lubrication. I. Lubricant flow visualization. Lubr Eng 48(2):96–104
120. Boning D, Lee B, Oji C, Ouma D, Park T, Smith T, Tugbawa T (1999) Pattern dependent modeling for CMP optimization and control. Materials Research Society (MRS) Spring Meeting. San Francisco, CA.
121. Runnels SR (1996) Advances in physically based erosion simulators for CMP. J Electron Mater 25(10):1574–1580
122. Nguyen V, VanKranenburg H, Woerlee P (2000) Dependency of dishing on polish time and slurry chemistry in Cu CMP. Microelectron Eng 50(1–4):403–410
123. Mpagazehe JN, Thukalil GA, Higgs III CF (2009) A study to estimate the number of active particles in CMP. Materials Research Society Spring Meeting. San Francisco, CA.
124. Edwards JK, McLaury BS, Shirazi SA (2001) Modeling solid particle erosion in elbows and plugged tees. J Energy Resourc Technol 123:277–284
125. Street KW, Marchetti M, Wal RLV, Tomasek AJ (2004) Evaluation of the tribological behavior of nano-onions in Krytox 143AB. Tribol Lett 16(1–2):143–149
126. Zantye PB, Kumar A, Sikder AK (2004) Chemical mechanical planarization for microelectronics applications. Mater Sci Eng R Rep 45(3–6):89–220
127. Nikas GK (2010) A state-of-the-art review on the effects of particulate contamination and related topics in machine-element contacts. Proc Inst Mech Eng J J Eng Tribol 224 (J5):453–479
128. Wang A, Essner A (2001) Three-body wear of UHMWPE acetabular cups by PMMA particles against CoCr, alumina and zirconia heads in a hip joint simulator. Wear 250:212–216
129. Chinas-Castillo F, Spikes HA (2003) Mechanism of action of colloidal solid dispersions. J Tribol 125(3):552–557
130. Lovell MR, Kabir MA, Menezes PL, Higgs CF III (2010) Influence of boric acid additive size on green lubricant performance. Philos Trans R Soc A 368:4851–4868
131. Duan B, Lei H (2001) The effect of particle size on the lubricating properties of colloidal polystyrene used as water based lubrication additive. Wear 249:528–532
132. Nikas GK, Sayles RS (2008) A study of lubrication mechanisms using two-phase fluids with porous bearing materials. Proc Inst Mech Eng J J Eng Tribol 222:771–783
133. Darley HCH, Gray GR (1988) Composition and properties of drilling and completion fluids, 5th edn. Butterworth-Heinemann, Houston, TX
134. Pepper S (2011) Effect of test environment on lifetime of two vacuum lubricants determined by spiral orbit tribometry. NASA, Cleveland, OH
135. Higgs CF, Ng ISH, Borucki L, Yoon I, Danyluk S (2005) A mixed-lubrication approach to predicting cmp fluid pressure modeling and experiments. J Electrochem Soc 152(3): G193–G198
136. Shan L, Levert J, Meade L, Tichy J, Danyluk S (2000) Interfacial fluid mechanics and pressure prediction in chemical mechanical polishing. J Tribol 122(3):539–543

137. Park S-S, Cho C-H, Ahn Y (2000) Hydrodynamic analysis of chemical mechanical polishing process. Tribol Int 33(10):723–730
138. Gohar R (1988) Elastohydrodynamics. Wiley, New York
139. Luo J, Dornfeld DA (2001) Mechanical removal mechanism in chemical mechanical polishing: theory and modeling. IEEE Trans Semicond Manuf 14(2):112–133
140. Terrell EJ, Higgs CF (2009) A particle-augmented mixed lubrication modeling approach to predicting chemical mechanical polishing. J Tribol 131(1):012201
141. Li Q, Rudolph V, Wang FY, Horio M (2005) A study of particle packing compression under fluid drag force by DEM simulations. Dev Chem Eng Miner Process 13(5–6):693–708
142. Mei R, Shang H, Walton OR, Klausner JF (2000) On the improved flowability of cohesive powders by coating with fine particles. Proc. of 1997 TMS Annual Meeting. pp. 225–236
143. Erdemir A (1994) Crystal chemistry and solid lubricating properties of the monochalcogenides gallium selenide and tin selenide. STLE Tribol Trans 37(3):471–478
144. Higgs CF, Heshmat H (2001) Characterization of pelletized MoS2 powder particle detachment process. ASME J Tribol 123(3):455–461
145. Higgs CF, Heshmat CA, Heshmat HS (1999) Comparative evaluation of MoS2 and WS2 as powder lubricants in high speed, multi-pad journal bearings. J Tribol Trans ASME 1–121 (3):625–630
146. Kaur RG, Higgs CF, Heshmat HS (2001) Pin-on disk tests of pelletized molybdenum disulfide. Tribol Trans 44(1):79–87
147. Heshmat H, Heshmat CA (1999) The effect of slider geometry on the performance of a powder lubricated bearing. Tribol Trans 42(3):640–646
148. Sawyer WG, Ziegert JC, Schmitz TL, Barton A (2006) In situ lubrication with boric acid: Powder delivery of an environmentally benign solid lubricant. Tribol Trans 49(2):284–290
149. Johnson VR, Lavik MT, Vaughn GW (1957) Mechanism of WS2 lubrication in vacuum. J Appl Phys 28(7):821
150. Kaur RG, Heshmat H (2002) 100 mm diameter self-contained solid/ powder lubricated auxiliary bearing operated at 30,000 rpm. Lubr Eng 58(6):13–20
151. Heshmat H (1992) Powder-lubricant piston ring for diesel engines. U.S. Patent, Editor E. Rollins Cross, United States
152. Reches Z, Lockner DA (2010) Fault weakening and earthquake instability by powder lubrication. Nature 467:452–455
153. Ettles CM (1985) The thermal control of friction at high sliding speed. ASME Paper 85
154. Heshmat H, Pinkus O, Godet M (1989) On a common tribological mechanism between interacting surfaces. Tribol Trans 32(1):32–41
155. Heshmat H, Godet M, Berthier Y (1995) On the role of and mechanism of dry triboparticulate lubrication. Lubr Eng 51(7):557–564
156. Heshmat H (1995) The quasi-hydrodynamic mechanism of powder lubrication: Part III On theory and rheology of triboparticulates. Tribol Trans 38(2):269–276
157. Higgs CF, Heshmat H (1999) Characterization of pelletized MoS2 powder particle detachment process. ASME J Tribol 123(3):640–646
158. Higgs CF, Wornyoh EYA (2007) An in situ mechanism for self-replenishing powder transfer films: Experiments and modeling. Wear 264:131–138
159. Heshmat H (1991) The rheology and hydrodynamics of dry powder lubrication. Tribol Trans 34(3):433–439
160. Iordanoff I, Berthier Y, Descartes S, Heshmat H (2002) A review of recent approaches for modeling solid third bodies. ASME J Tribol 124(4):725–735
161. Dai FL, Khonsari MM, Lu ZY (1994) On the lubrication mechanism of grain flows. Tribol Trans 37(3):516–524
162. Mckeague KT, Khonsari MM (1996) Generalized boundary interactions for powder lubricated couette flows. ASME J Tribol 118(3):580–588
163. Yu CM, Craig K, Tichy J (2005) Granular collision lubrication. J Rheol 38(4):921–936
164. Fillot N, Iordanoff I, Berthier Y (2005) Simulation of wear through mass balance in a dry contact. ASME J Tribol 127(1):230–237

Problems

12.1 *Single Particle Coefficient of Restitution Analysis*
Understanding granular flow tribology hinges on an understanding of the interactions of individual particles at the local level. As discussed in the chapter, one of the key parameters at the local particle interaction level is the coefficient of restitution. Evaluate each of the following problems related to the coefficient of restitution:

(a) Find e for the collision of a sphere falling from rest at an initial height of 18 in., which collides with a stationary plate and rebounds at a velocity of 2.43 m/s.
(b) Assuming a sphere colliding with a stationary block, derive an expression for the coefficient of restitution (e), in terms of the pre-collision (KE_i) and post-collision kinetic energy (KE_r) of the sphere.
(c) In experiments, it is impossible to study the effects of certain individual particle properties, such as material density (ρ), due to the inability to experimentally vary them in isolation. This is where modeling, theoretical and/or FEM, can become particularly useful. Consider a sphere (granule) being dropped from rest against a stationary block. Under a certain set of collision conditions, the coefficient of restitution (e_1) between the sphere and the block is found to be 0.85. Now consider a second collision case, where *only* the material density of the sphere (ρ_s) was to change and be increased by a factor of 1.5. Assuming all other parameters of the collision remain the same, use the theoretical formulation (12.5) to predict the coefficient of restitution (e_2) for this second collision case.

12.2 *Particle Settling*
You are a tribologist working for a chemical plant and are responsible for a new process. During this process, a small amount of nickel catalyst particles (100 μm in diameter) are placed into a 15 m-tall vat of vegetable oil to encourage a chemical reaction. Though the suspension is very dilute, it has been found that the catalyst particles cause substantial erosive and abrasive wear to downstream equipment. As a result, the oil must be particle-free before it can be sent to downstream processing equipment. Using gravitational settling would be significantly less expensive than filtering the catalyst particles out of the oil. The maximum amount of time the plant operators can wait for the particles to settle is 2 h. Calculate whether or not gravitational settling will be a viable method of separating the catalyst particles from the vegetable oil given the time constraints of the plant operators.

12.3 *Derivation of Powder Equation*
Derive (12.25) starting from (12.22).

12.4 *Powder Film Classification*
What is the difference between thick film powder lubrication and thin film powder lubrication?

Solutions

12.1 Part a:. *Solution.*

$$v_{imp}^2 = v_I^2 + 2gH_I = 0^2 + 2(9.81m/s)(18in.)(0.0254m/in.) = 8.970m^2/s^2$$
$$v_{imp} = -2.995m/s$$

From (12.2):

$$e = \frac{-v_{reb}}{v_{imp}} = \frac{-2.43m/s}{-2.995m/s}$$
$$e = 0.81$$

Part b:. Starting from (12.1)

$$e = \frac{v_{reb,1} - v_{reb,2}}{v_{imp,2} - v_{imp,1}}$$

Assuming the stationary block is object 1 and the sphere is object 2, this can be reduced to

$$e = \frac{0 - v_{reb,2}}{v_{imp,2} - 0} = \frac{-v_{reb,2}}{v_{imp,2}} \tag{1}$$

Just before impact the sphere's kinetic energy is given by

$$KE_{imp,2} = \frac{1}{2}mv_{imp,2}^2$$

Solving for the impact velocity gives

$$v_{imp,2} = \sqrt{\frac{2KE_{imp,2}}{m}} \tag{2}$$

Similarly the rebound velocity of the sphere can be derived in terms of kinetic energy as

$$v_{reb,2} = \sqrt{\frac{2KE_{reb,2}}{m}} \tag{3}$$

Substituting (2) and (3) into (1) yields

$$e = \frac{-\sqrt{\frac{2KE_{reb,2}}{m}}}{\sqrt{\frac{2KE_{imp,2}}{m}}} = -\sqrt{\frac{KE_{reb,2}}{KE_{imp,2}}}$$

Using KE_i and KE_r to represent the pre-collision and post-collision kinetic energy of the sphere and since the positive or negative root can be obtained, this can simply be written as

$$e == \sqrt{\frac{KE_r}{KE_i}}$$

Part c:. First, derive e as a function of ρ_s. Start from (12.5):

$$e = 1.88\left(\frac{p_d}{E^*}\right)^{\frac{1}{2}}\left(\frac{\frac{1}{2}m_s v_{imp}^2}{p_d R^3}\right)^{-\frac{1}{8}} \tag{1}$$

Consider the equation for the reduced radius of curvature between the sphere and block:

$$\frac{1}{R} = \frac{1}{R_s} + \frac{1}{R_{block}},$$

where $R_{block} \to \infty$
Solving for R yields

$$\frac{1}{R} = \frac{1}{R_s} + \frac{1}{\infty} = \frac{1}{R_s} + 0 = \frac{1}{R_s}$$
$$R = R_s \tag{2}$$

Substitute (2) into (1) to obtain

$$e = 1.88\left(\frac{p_d}{E^*}\right)^{\frac{1}{2}}\left(\frac{\frac{1}{2}m_s v_{imp}^2}{p_d {R_s}^3}\right)^{-\frac{1}{8}} \tag{3}$$

The density of the sphere (ρ_s) can be written as

$$\rho_s = \frac{m_s}{V_s} = \frac{m_s}{\frac{4}{3}\pi R_s^3}$$

Rearranging this expression yields

$$\frac{m_s}{R_s^3} = \frac{4}{3}\pi\rho_s \tag{4}$$

Substitute (4) into (3) to obtain

$$e = 1.88\left(\frac{p_d}{E^*}\right)^{\frac{1}{2}}\left(\frac{\frac{1}{2}\frac{4}{3}\pi\rho_s v_{imp}^2}{p_d}\right)^{-\frac{1}{8}} = 1.88\left(\frac{p_d}{E^*}\right)^{\frac{1}{2}}\left(\frac{\frac{2}{3}\pi\rho_s v_{imp}^2}{p_d}\right)^{-\frac{1}{8}}$$

Since no parameters (besides ρ_s) change between the two collision cases (1 and 2) defined in the problem, this expression can be written for the two collision cases as

$$e_1 = C\rho_{s1}^{-1/8}$$
$$e_2 = C\rho_{s2}^{-1/8}$$

In these equations, C is a constant which is equivalent in the two equations. From this, it can be obtained that

$$C = \frac{e_1}{\rho_{s1}^{-1/8}} = \frac{e_2}{\rho_{s2}^{-1/8}} \tag{5}$$

It is given in the problem that

$$e_1 = 0.85 \tag{6}$$

$$\rho_{s2} = 1.5\rho_{s1} \tag{7}$$

Substitute (6) and (7) into (5) to obtain

$$\frac{0.85}{\rho_{s1}^{-1/8}} = \frac{e_2}{(1.5\rho_{s1})^{-1/8}}$$

Solve for e_2:

$$0.85(1.5\rho_s)^{-1/8} = e_2\rho_{s1}^{-1/8}$$
$$0.85(1.5)^{-1/8}\rho_{s1}^{-1/8} = e_2\rho_{s1}^{-1/8}$$
$$0.85(1.5)^{-1/8} = e_2$$
$$e_2 = 0.81$$

12.2 The particles in the suspension will have a number of different forces acting on them. By using Newton's second law (12P.1), it is possible to estimate when they will fall out of suspension.

$$\boldsymbol{F} = m\boldsymbol{a} \tag{12P.1}$$

Because a clue is provided in the problem that the suspension is very dilute, surface forces between particles are neglected. As a result, the primary forces acting on the particles are gravity, buoyancy, and drag. The force of gravity $\boldsymbol{F_g}$ is calculated from (12P.1) where ρ_p is the particle density, V is the particle volume, and $\boldsymbol{g}$ is the gravitational acceleration.

$$\boldsymbol{F_g} = \rho_p \boldsymbol{g} V \tag{12P.2}$$

The force of buoyancy on the particle is based on the particle volume and can be calculated using (12P.3), where ρ_f is the fluid density.

$$\boldsymbol{F_b} = \rho_f \boldsymbol{g} V \tag{12P.3}$$

The force of drag acting on the particles can be calculated using a Stokes drag formulation based on the assumption that the Reynolds number, Re, is significantly less than unity. If this is the case, the force of drag can be calculated from (12.19)

$$\boldsymbol{F}_{drag} = 6\pi\eta \boldsymbol{U} a \tag{12.19}$$

It is important to note here that U is equal to the difference between the particle velocity and the fluid velocity.

$$\boldsymbol{U} = \boldsymbol{U_p} - \boldsymbol{U_f}$$

Because the fluid is mostly stationary, the fluid velocity will be considered zero. Particles falling out of suspension will reach a constant terminal velocity in which the sum of all forces on them is zero. Using this information to populate (12P.1), (12P.4) can be generated.

$$\begin{aligned} \boldsymbol{F}_{drag} &= \boldsymbol{F}_g - \boldsymbol{F}_b \\ 6\pi\eta U a &= \rho_p \boldsymbol{g} V - \rho_f \boldsymbol{g} V \\ U_p &= \frac{V \boldsymbol{g} \left(\rho_p - \rho_f\right)}{6\pi\eta a} \end{aligned} \tag{12P.4}$$

Continuing the assumption that the particles are spherical, the volume can be calculated as

$$V = \frac{4}{3}\pi a^3$$

The resulting equation can be used to calculate the terminal velocity of the particle

$$U_p = \frac{4\boldsymbol{g}\left(\rho_p - \rho_f\right)}{18\eta} a^2 \tag{12P.5}$$

Inserting values for the variables

Gravitational acceleration $\boldsymbol{g} = -9.81\ \mathrm{m/s^2}$

Density of the particles $\rho_p = 8{,}908$ kg/m^3
Density of the fluid $\rho_p = 918.8$ kg/m^3
Viscosity of the fluid $\eta = 0.0523$ Pa s
Radius of the particles a = 50E−6 m
yields a terminal velocity of −0.00083 m/s

This velocity is based upon the assumption that Stokes drag (12.19) would be valid for this scenario. To check the validity of this assumption, we check the Reynolds number using of the calculated particle velocity:

$$Re = \frac{\rho_f U_p 2a}{\eta}$$
$$Re = 0.00147$$

It is seen, that the Reynolds number is significantly less than unity and the use of the Stokes drag formulation was appropriate. Dividing the height of the tank, 15 m, by the terminal velocity of the particles means that the particles will take a minimum of approximately 5 h to fall out of suspension. The particles will actually take longer due to the time needed for them to accelerate to their terminal velocity. This time frame will be too long for the chemical plant and a different type of particle separation will be desired:

12.3 *Start with* $\dot{S} = \dot{I} - O$

$$\dot{S} = \frac{dV}{dt} \text{ and } V = A \text{ (area)} \times h \text{ (height) so, } \dot{S} = A\frac{dh}{dt}$$

$$\dot{I} = K_p F_p U \text{ (applying Eq.(12.23) at pellet/disk interface)}$$
$$\dot{O} = K_{es} F_s U \text{ (applying Eq.(12.23) at slider/disk interface)}$$

There is one more output rate which is caused by the pellet at the pellet/disk interface.

So, $\dot{O} = K_{ep} F_p U + K_{es} F_s U$

After applying the linear rule of mixture, we arrive at Eq. (12.24)

$$A\frac{dh}{dt} = K_p F_p U\ (1 - X) - \left(K_{ep} F_p U + K_{es} F_s U\right)(X)$$

We know that $X = \frac{h}{h_{\max}}$ *from Eq.*(12.21). *We can substitute h with X in the storage rate.*

Eq.(12.24) *becomes* :

$$A\ h_{\max}\frac{dX}{dt} = K_p F_p U\ (1 - X) - \left(K_{ep} F_s U + K_{es} F_s U\right)(X)$$

Solving the differential equation u sin g integrating factor method:

$$X(t) = \frac{K_p F_p}{K_p F_p + K_{ep} F_p + K_{es} F_s} - \frac{K_p F_p}{K_p F_p + K_{ep} F_p + K_{es} F_s} \exp\left(- \frac{\left(K_p F_p + K_{ep} F_p + K_{es} F_s\right) \ U \ t}{A \ h_{\max}} \right)$$

Simplify and define τ (time cons tan t), we arrive at Eq. (12.25)

12.4 Thick film powder lubrication is when the powder film separates the two interacting surfaces completely so that no contact occurs between them. The film height extends beyond the highest asperity. Typically, this phenomenon is associated with hydrodynamic lubrication, and that is when the rubbing surfaces are separated due to the hydrodynamic lift generated by the film flowing through a converging gap. Thin film powder lubrication is when the powder film does not extend beyond the highest asperity, and there is a constant contact between the two interacting surfaces. This phenomenon is often associated with boundary lubrication.